Thesis for the degree of Doctor of Philosophy

# Impurity transport in magnetically confined fusion plasmas

Albert Mollén


CHALMERS

Department of Applied Physics
Chalmers University of Technology
Göteborg, Sweden, 2015

Impurity transport in magnetically confined fusion plasmas
Albert Mollén



ISBN 978-91-7597-192-6

Doktorsavhandlingar vid Chalmers tekniska högskola
Ny serie Nr 3873
ISSN 0346-718X

Nuclear Engineering
Department of Applied Physics
Chalmers University of Technology
SE–412 96 Göteborg
Sweden
Telephone +46–(0)31–772 10 00

Some figures in this thesis are in color only in the electronic version, available online through Chalmers Publication Library.

Cover:
The image illustrates the impurity distribution in a shot from the Alcator C-Mod tokamak when applying ICRH, courtesy of M. L. Reinke.
See p. 43 for more details.

Printed in Sweden by
Reproservice
Chalmers Tekniska Högskola
Göteborg, Sweden, 2015

Impurity transport in magnetically confined fusion plasmas
Albert Mollén
Department of Applied Physics
Chalmers University of Technology

## Abstract

Nuclear fusion is foreseen as one of the options for future energy production. In establishing the physics basis of future magnetic fusion reactors it is necessary to find scenarios where the impurity content in the core can be kept low. High concentration of impurities leads to dilution and radiative energy losses and is detrimental for fusion reactivity. Therefore the understanding and control of impurity transport is of critical importance for the success of fusion. Impurity transport in fusion plasmas is often dominated by turbulent fluctuations, but in certain scenarios, and in particular for 3D magnetic configurations, the collisional contribution can be significant. This thesis addresses the effect of poloidal asymmetries on turbulent impurity transport in axisymmetric devices (tokamaks), and collisional impurity transport in 3D configurations (stellarators). In tokamaks, transport driven by ion temperature gradient mode and trapped electron mode turbulence is studied through gyrokinetic modelling. It is shown that poloidal asymmetries can significantly affect radial transport, and could contribute in reducing the impurity core content. The theoretical predictions are compared to experimental data from the Alcator C-Mod tokamak, where poloidal asymmetries are induced by radiofrequency heating. Furthermore, we show that collisional transport in stellarators can cause very strong impurity accumulation, highlighting this as one of the major concerns for 3D devices as a reactor concept. We also investigate how the bootstrap current is affected by the presence of impurities.

**Keywords:** fusion plasma physics, tokamak, stellarator, transport, drift-kinetic, gyrokinetic, turbulence, impurity, poloidal asymmetry

# Publications

This thesis is based on the work contained in the following papers:

[A] A. Mollén, I. Pusztai, T. Fülöp, Ye. O. Kazakov and S. Moradi. Effect of poloidal asymmetries on impurity peaking in tokamaks. *Phys. Plasmas* **19**, 052307 (2012). http://dx.doi.org/10.1063/1.4719711.

[B] I. Pusztai, A. Mollén, T. Fülöp and J. Candy. Turbulent transport of impurities and their effect on energy confinement. *Plasma Phys. Control. Fusion* **55**, 074012 (2013). http://dx.doi.org/10.1088/0741-3335/55/7/074012.

[C] A. Mollén, I. Pusztai, T. Fülöp and S. Moradi. Impurity transport in trapped electron mode driven turbulence. *Phys. Plasmas* **20**, 032310 (2013). http://dx.doi.org/10.1063/1.4796196.

[D] I. Pusztai, M. Landreman, A. Mollén, Ye. O. Kazakov and T. Fülöp. Radio frequency induced and neoclassical asymmetries and their effects on turbulent impurity transport in a tokamak. *Contrib. Plasma Phys.* **54**, 534 - 542 (2014). http://dx.doi.org/10.1002/ctpp.201410012.

[E] A. Mollén, I. Pusztai, M. L. Reinke, Ye. O. Kazakov, N. T. Howard, E. A. Belli, T. Fülöp and The Alcator C-Mod Team. Impurity transport in Alcator C-Mod in the presence of poloidal density variation induced by ion cyclotron resonance heating. *Plasma Phys. Control. Fusion* **56**, 124005 (2014). http://dx.doi.org/10.1088/0741-3335/56/12/124005.

[F] A. Mollén, M. Landreman and H. M. Smith. On collisional impurity transport in nonaxisymmetric plasmas.
*J. Phys.: Conf. Ser.* **561**, 012012 (2014).
http://dx.doi.org/10.1088/1742-6596/561/1/012012.

[G] A. Mollén, M. Landreman, H. M. Smith, S. Braun and P. Helander. Impurities in a non-axisymmetric plasma: transport and effect on bootstrap current.
Submitted to *Phys. Plasmas*.

## Statement of contribution

I performed the simulations, data analysis and presentation for papers A, C, F and G. I was the main contributor in understanding the results of these simulations, preparing the figures and writing most of the text. In papers B and D I verified the semi-analytical models introduced by the first author, and helped preparing parts of the results. In paper E I conducted the numerical analysis of the experimental data from the studied discharge. I prepared most of the figures and was responsible for writing the main part of the manuscript.

## Additional publications (not included in the thesis)

[H] S. Moradi, T. Fülöp, A. Mollén and I. Pusztai. A possible mechanism responsible for generating impurity outward flow under radio frequency heating.
*Plasma Phys. Control. Fusion* **53**, 115008 (2011).
http://dx.doi.org/10.1088/0741-3335/53/11/115008.

[I] S. Moradi, I. Pusztai, A. Mollén and T. Fülöp. Impurity transport due to electromagnetic drift wave turbulence.
*Phys. Plasmas* **19**, 032301 (2012).
http://dx.doi.org/10.1063/1.3688876.

[J] S. Moradi, I. Pusztai, W. Guttenfelder, T. Fülöp and A. Mollén. Microtearing modes in spherical and conventional tokamaks.
*Nucl. Fusion* **53**, 063025 (2013).
http://dx.doi.org/10.1088/0029-5515/53/6/063025.

[K] M. Landreman, H. M. Smith, A. Mollén and P. Helander. Comparison of particle trajectories and collision operators for collisional transport in nonaxisymmetric plasmas.
*Phys. Plasmas* **21**, 042503 (2014).
http://dx.doi.org/10.1063/1.4870077.

[L] T. Fülöp, S. Moradi, A. Mollén and I. Pusztai. The role of poloidal asymmetries in impurity transport.
In *Europhysics Conference Abstracts*, volume 35G, page P2.114, Strasbourg, France, 2011.
http://ocs.ciemat.es/EPS2011PAP/pdf/P2.114.pdf.

[M] S. Moradi, T. Fülöp, A. Mollén and I. Pusztai. Possible mechanism responsible for generating impurity outward flow under radio frequency heating.
In *14*$^{\text{th}}$ *European Fusion Theory Conference*, Frascati, Italy, 2011.
http://www.fusione.enea.it/EVENTS/eventifiles/EFTC14-2011/Posters/PRESENTAZIONI%20POSTER/MORADI.pdf.

[N] A. Mollén, I. Pusztai, T. Fülöp, Ye. O. Kazakov and S. Moradi. Effect of poloidal asymmetries on impurity peaking in tokamaks. In *Europhysics Conference Abstracts*, volume 36F, page P4.028, Stockholm, Sweden, 2012. http://ocs.ciemat.es/EPSICPP2012PAP/pdf/P4.028.pdf.

[O] S. Moradi, I. Pusztai, T. Fülöp and A. Mollén. Impurity transport due to electromagnetic drift wave turbulence. In *24*$^{\text{th}}$ *IAEA Fusion Energy Conference*, San Diego, USA, 2012. http://www-naweb.iaea.org/napc/physics/FEC/FEC2012/html/proceedings.pdf.

[P] A. Mollén, I. Pusztai, T. Fülöp, S. Moradi, M. L. Reinke and Ye. Kazakov. Impurity peaking in tokamaks. In *Europhysics Conference Abstracts*, volume 37D, page P4.138, Espoo, Finland, 2013. http://ocs.ciemat.es/EPS2013PAP/pdf/P4.138.pdf.

[Q] A. Mollén, I. Pusztai, M. L. Reinke, Ye. O. Kazakov, N. T. Howard and T. Fülöp. Impurity transport in Alcator C-Mod in the presence of poloidal density variation induced by ion cyclotron resonance heating. In *Europhysics Conference Abstracts*, volume 38F, page P5.043, Berlin, Germany, 2014. http://ocs.ciemat.es/EPS2014PAP/pdf/P5.043.pdf.

# Contents

# Acknowledgments

There are many people to thank for supporting me throughout my years of PhD studies. Firstly, this work would not have been possible without my supervisors Prof. Tünde Fülöp and Dr. István Pusztai. Tünde is a most dedicated person who strives to get the best possible out of her students. With her deep knowledge she has been an exceptional guidance to me during the start of my academic career. István is a living encyclopedia in the transport field; I have never had a question he was not able to answer. At the same time he is the most helpful person I can imagine and has contributed substantially to my work.

In the later stages of my studies I have had the pleasure to work with Dr. Matt Landreman from University of Maryland and Dr. Håkan Smith from Max Planck Institute for Plasma Physics. This has been extremely fruitful for my own development and I hope we can continue our collaboration in the future. I would also like to thank Prof. Per Helander from Max Planck Institute for Plasma Physics and Dr. Jeff Candy from General Atomics who invited me to visit their research institutes for longer periods, something I have benefited greatly from. Moreover, I thank Dr. Matthew Reinke for his help with providing experimental data.

During my days at the office I have come across several interesting companions. Adam, Eero, Emelie, Geri, Ola, Sara, Yevgen, thanks for making research much more of a pleasure. I also direct my gratitude to my colleagues at the division of Nuclear Engineering at the Applied Physics department, with whom I have enjoyed an innumerable number of coffee breaks.

# Abbreviations

## Acronyms

| | |
|---|---|
| GK | **G**yro**K**inetic |
| ICRH | **I**on **C**yclotron **R**esonance **H**eating |
| ITG | **I**on **T**emperature **G**radient |
| MHD | **M**agneto**H**ydro**D**ynamic(s) |
| RF | **R**adio**F**requency |
| TE | **T**rapped **E**lectron |
| FLR | **F**inite **L**armor **R**adius |

## Tokamaks

| | |
|---|---|
| ITER | **I**nternational **T**hermonuclear **E**xperimental **R**eactor<br>("The Way" in Latin),<br>Under construction in Cadarache, France. |
| JET | **J**oint **E**uropean **T**orus,<br>Culham Science Centre, Abingdon, UK. |
| JT-60U | Naka, Japan. |
| Alcator C-Mod | MIT, Cambridge MA, USA. |
| ASDEX Upgrade | Garching, Germany. |

## Stellarators

| | |
|---|---|
| W7-X | **W**endelstein 7-X,<br>Max-Planck-Institut für Plasmaphysik (IPP),<br>Under construction in Greifswald, Germany. |
| LHD | **L**arge **H**elical **D**evice,<br>National Institute for Fusion Science,<br>Toki, Gifu, Japan. |

# Chapter 1

# Introduction

At the present, mankind is in a period of increasing demand for energy production. All existing energy sources have their drawbacks, and the search for new sustainable alternatives is one of our most important challenges. Many of today's most utilized technologies put large loads on the environment, and global warming is an evident reality [1].

Thermonuclear fusion is a possible candidate to become a long-term option to meet our requirements on energy production. Fusion is the harvest of the high energy content of atomic nuclei, by extracting the energy released when light nuclei combine into heavier ones. In contrast, existing nuclear reactors implement fission which means splitting heavy nuclei into lighter ones. Fusion has many advantages over fission, especially with respect to safety and radioactive waste, but remains unrealized as a reactor concept even though the idea is about 90 years old [2]. Still the effect of fusion is everywhere around us since it is the process which generates the energy of the Sun and the stars. The reason why energy production through fusion on Earth is complicated stems from the high temperatures required to maintain the fusion reactions. The most feasible fusion reaction is between the heavier isotopes of hydrogen, deuterium and tritium [3]:

$$\mathrm{D} + \mathrm{T} \rightarrow {}^{4}\mathrm{He} + \mathrm{n} + 17.6\ \mathrm{MeV}.$$

To overcome the Coulomb repulsion between the positively charged nuclei, and sustain the process with a reasonable efficiency, requires a temperature of $\sim 10^8\,\mathrm{K}$. At this high temperature atoms and molecules are no longer intact, and the medium enters the plasma state of matter consisting of free ions and electrons.

There are three ways to control a fusion plasma. The stars use the gravitational force to confine the plasma, but this method is not practical on Earth. The second method is to compress small fuel pellets to high densities with ultra-intense lasers and utilize the inertia of the matter to confine the plasma. This is called inertial confinement. Although a few countries conduct research in this area there is skepticism about its practicality and cost-effectiveness. The method commonly believed to be the main candidate is instead magnetic confinement.

Magnetic confinement of fusion plasmas takes advantage of the fact that the particles of plasmas are charged, and can therefore be controlled by magnetic fields through the Lorentz force. The only three-dimensional topology with non-vanishing continuous tangent vector field is the torus. Accordingly, to prevent high losses, many magnetic confinement devices have toroidal geometries. To date the most successful device is the tokamak with an axisymmetric twisted magnetic field (up to $\sim 10$ T), created by external coils and an induced plasma current (of the order of a few MA). The twist is necessary in order to avoid losses through particle drifts.

One of the main indicators of how well a fusion device performs is the achieved value of the fusion triple product $n_i T_i \tau_{\mathrm{E}}$, which is the product of the ion density and temperature (i.e. ion pressure) together with the energy confinement time, $\tau_{\mathrm{E}}$. The latter is a measure of how long energy, created from fusion reactions, stays in the plasma and a high enough value is required for the fusion reaction to be self-sustained. The tokamak holding the current world record for highest fusion triple product is the JT-60U experiment in Japan [4]. However, the tokamak with the largest produced fusion power is JET in the UK, which in 1997 produced 16 MW of fusion power – 65% of the input power. JET is also the largest existing fusion experiment. The next step for the magnetic confinement fusion community is ITER, under construction in Cadarache, France. It will be an even bigger experiment with the overall goal to demonstrate the technical feasibility of fusion energy production, and is expected to produce 500 MW fusion power from 50 MW input power [5, 6].

To improve confinement, and by that increase the energy confinement time, the radial particle and energy fluxes should be minimized. The magnetic field lines of a tokamak trace out nested toroidal flux surfaces and a charged particle, if it would not interact with other charged particles, will always be in the close vicinity of a certain flux surface.

However due to the long range nature of the Coulomb force, the charged particles will always interact with each other through Coulomb collisions. The early way of describing transport processes in tokamaks was through a diffusive model based on the Coulomb interaction, the "neoclassical" transport model [7]. From experiments it was soon realized that this model only describes an irreducible minimum to the level of transport experienced in tokamaks, and typically it is overshadowed by a larger transport due to plasma turbulence. Plasma turbulence can be generated through various kinds of small-scale low-frequency fluctuations, referred to as microinstabilities, which are driven by the density and temperature gradients. The theory of plasma turbulence is a complex and nonlinear field, with models of different degrees of sophistication. Purely analytical models are too coarse to give a satisfactory explanation and one has to resort to nonlinear kinetic simulation codes. This field has experienced fast progress in recent years, together with the rapid increase of computer performance and development of supercomputers. Nevertheless, reduced models are still important to understand underlying physical mechanisms and ease the interpretation of simulation results.

Besides analyzing the radial fluxes of the main plasma species (i.e. fuel ions and electrons) it is also desirable to describe the behavior of impurity ion species. Impurities are ubiquitous in fusion plasmas, foremost in the form of alpha particles ($^4He^{2+}$) which are a rest product of the D-T fusion reaction, but impurities of higher charge can also enter the plasma by sputtering, arcing and evaporation of the surrounding wall surface, or even artificially by impurity seeding. The presence of impurities leads to plasma dilution and radiative energy losses, and therefore results in a degradation of fusion performance. Impurities of high charge are especially detrimental, mainly because radiation losses are proportional to the square of the charge number, $Z^2$ [3]. The impurity concentration is typically low compared to the main species, but even a small content can cause severe problems if $Z$ is high. In a steady state, the particle density profiles of a tokamak are usually peaked, meaning that the density is highest in the core and decreases in the radial direction. This is also often true for the impurity species. Since the core is the location where most fusion reactions take place (the temperature is also highest in the core) it is undesirable to have impurities accumulating there. In contrast, at the plasma edge impurities can be beneficial for mitigation of the heat loads on the surrounding walls. Consequently it is interest-

ing to look for scenarios where impurities are transported out of the core into the edge region.

The remainder of the thesis is organized as follows. In Chapter 2 an introduction to the theory of magnetized toroidal fusion plasmas is given. We introduce the tokamak and stellarator concepts for plasma confinement. Then kinetic transport theory for magnetized fusion plasmas is discussed in Chapter 3. The drift-kinetic and gyrokinetic approaches are introduced, and how they apply to collisional and turbulent cross-field transport of particles and energy. Finally in Chapter 4 we summarize the papers and conclude.

# Chapter 2

# Basic theory of magnetized toroidal fusion plasmas

The aim of the present chapter is to introduce some fundamental concepts of plasmas, and in particular of toroidally shaped fusion plasmas in strong magnetic fields.

## 2.1 Magnetized fusion plasmas

A plasma consists of charged particle species, electrons and ions (not necessarily fully ionized), which on a macroscopic level balance each other according to the quasi-neutrality condition [8]

$$n_e = \sum_i Z_i n_i. \tag{2.1}$$

Here $n_e$ is the electron density while $n_i$ and $Z_i$ are the particle density and charge of ion species $i$ (including impurity ions). This condition is valid on length scales significantly larger than the electron Debye length $\lambda_{De} = \sqrt{\epsilon_0 T_e / e^2 n_e}$ and for time scales longer than the inverse plasma frequency $\omega_{pe}^{-1} = \sqrt{m_e \epsilon_0 / e^2 n_e}$, where $e$ is the electron charge, $m_e$ the electron mass, $T_e$ the electron temperature and $\epsilon_0$ the vacuum permittivity. For the center of a typical fusion plasma, where the temperature is $T_e \sim 10$ keV and the density $n_e \sim 10^{20}$ m$^{-3}$, these quantities can be of the order $\lambda_{De} \sim 10^{-4}$ m and $\omega_{pe}^{-1} \sim 10^{-11}$ s.

Out of all possible nuclear fusion reactions, the one with the largest cross section at reasonably achievable temperatures is that between deuterium (D) and tritium (T), the heavier isotopes of hydrogen [3]. Be-

cause of this, future fusion reactors are expected to operate with D-T fuel. However due to the radioactive properties of T and the difficulty of handling it, most fusion plasma experiments today use a single main ion species which is usually either deuterium or ordinary hydrogen. In transport theory it is consequently customary to assume that the main ion species is of charge $Z_i = 1$. Experimentally there will always be an amount of other ions present in the plasma, referred to as impurities, which can enter as a rest product of the fusion reactions or through plasma interaction with the surrounding wall. These impurity species are normally in significantly smaller quantities than the main species, but can still have a major impact on the plasma. It is useful to introduce a measure of the purity of the plasma, and this is referred to as the effective ion charge $Z_{\text{eff}} = \sum_i Z_i^2 n_i/n_e$. For a pure hydrogenic plasma $Z_{\text{eff}} = 1$, and it increases with the impurity content. The Bremsstrahlung radiation losses are directly proportional to $Z_{\text{eff}}$, and because of this the presence of high-$Z$ impurities, even in small quantities, can lead to severe energy losses through radiation. Moreover impurities also dilute the plasma, and together these effects can result in a heavy degradation of fusion reactivity.

## 2.2 Charged particle motion in strong magnetic fields

The motion of charged particles in a strong magnetic field is characterized by rapid gyration around the magnetic field lines. In a homogeneous magnetic field of strength $B$, the gyration frequency of species $\alpha$ is given by $\Omega_\alpha = e_\alpha B/m_\alpha$, and is consequently a function of charge and mass [7]. The Larmor radius of the gyration is $\rho_\alpha = v_\perp/\Omega_\alpha$, where $v_\perp$ denotes the magnitude of the particle velocity component perpendicular to the magnetic field. In this thesis, the subscripts $_\perp$ and $_\parallel$ represent perpendicular and parallel with respect to the magnetic field. In a strongly magnetized plasma the Coulomb collision frequency of species $\alpha$ should be much smaller than the gyro-frequency, $\nu_\alpha \ll \Omega_\alpha$, and the ion Larmor radius ($\rho_e \ll \rho_i$) should be much smaller than the characteristic length scale on which equilibrium plasma parameters vary (e.g. the density scale length $L_{n\alpha} = |\nabla \ln n_\alpha|^{-1}$ or temperature scale length $L_{T\alpha} = |\nabla \ln T_\alpha|^{-1}$), $\rho_i \ll L$. We will show later that these assumptions permit expansions in the smallness of certain parameters,

useful in transport theory.

It is convenient to decompose the particle position into the *guiding center* position and the *gyroradius* vector, $\mathbf{r} = \mathbf{R} + \mathbf{b} \times \mathbf{v}/\Omega_\alpha \equiv \mathbf{R} + \boldsymbol{\rho}$ with $\mathbf{b} = \mathbf{B}/B$. In a homogeneous magnetic field the guiding center motion will simply be given by $\dot{\mathbf{R}} = v_\parallel \mathbf{b}$, where $v_\parallel$ is the magnitude of the particle velocity component parallel to the magnetic field. In spatially varying magnetic fields and in the presence of electric fields, perpendicular drifts and the magnetic mirror force arise. The perpendicular drift velocity can be written

$$\mathbf{v}_d = \dot{\mathbf{R}}_\perp = \frac{\mathbf{E} \times \mathbf{B}}{B^2} + \frac{v_\perp^2}{2\Omega_\alpha} \mathbf{b} \times \nabla \ln B + \frac{v_\parallel^2}{\Omega_\alpha} \mathbf{b} \times \boldsymbol{\kappa}, \tag{2.2}$$

where the derivation assumes that the drift velocity is small compared to the particle velocity, $|\mathbf{v}_d| \ll |\mathbf{v}|$. Here $\boldsymbol{\kappa} = -\mathbf{b} \times (\nabla \times \mathbf{b})$ is the curvature vector of the magnetic field. The first term in Eq. (2.2) is the $\mathbf{E} \times \mathbf{B}$ drift velocity, independent of the particle charge and mass. The other two terms together represent the magnetic drift velocity due to inhomogeneities in the magnetic field, composed of the grad-$B$ drift and the curvature drift. Because of their $1/\Omega_\alpha$ dependence they depend on the particle charge and mass, and are in opposite directions for electrons and ions.

The magnetic mirror force acts in the direction parallel to the magnetic field and its magnitude is $\mu \nabla_\parallel B$, where $\mu = m_\alpha v_\perp^2 / (2B)$ is the magnetic moment of the gyrating particle. The force arises because the magnetic moment is an adiabatic invariant, meaning that over slow spatial and temporal changes of magnetic field strength the particle velocity will change to keep $\mu$ constant. This combined with the preservation of the total particle energy $\mathcal{E} = m_\alpha v^2/2 + e_\alpha \phi$, with $\phi$ being the electrostatic potential, results in a force in the direction opposite to the parallel gradient of $B$.

## 2.3 Magnetic geometry

A toroidal magnetic fusion device should confine a plasma with a pressure $p$ by using a magnetic field $\mathbf{B}$. The magnetic field closely describes an ideal toroidal magnetohydrodynamic (MHD) equilibrium [9], where the pressure is balanced by a magnetic force according to

$$\mathbf{j} \times \mathbf{B} = \nabla p, \tag{2.3}$$

where $\mathbf{j}$ is the total current density. From this equation it follows immediately that $\mathbf{B}$ and $\mathbf{j}$ lie in surfaces of constant pressure, $\mathbf{B}\cdot\nabla p = \mathbf{j}\cdot\nabla p = 0$. For plasma confinement, it is desirable that these surfaces are nested, i.e. lie inside each other, and the innermost surface is then simply a line called the magnetic axis. The surfaces, traced out by the magnetic field lines, are referred to as *flux surfaces* (this concept is illustrated in Fig. 2.1). In the usual situation the density and temperature of each species are approximately constant over a flux surface. However, as will be further discussed in this thesis, there are physical phenomena (e.g. plasma rotation and RF heating) that can cause significant asymmetries to arise for certain species. High-$Z$ impurities are especially prone due to their large charge and mass.

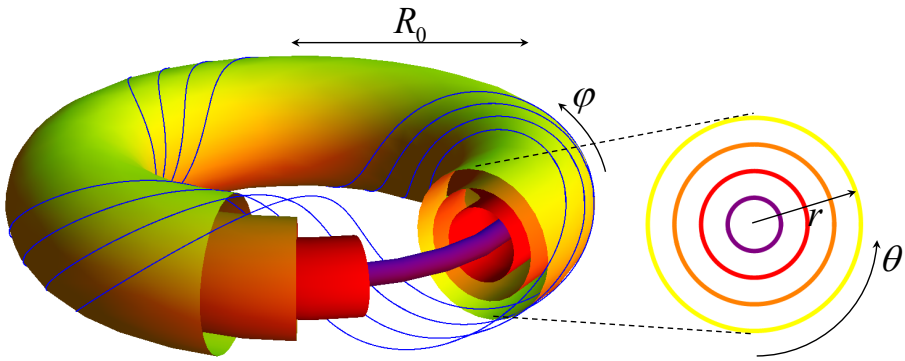


**Figure 2.1:** Toroidal geometry, with the parameters $(r, \theta, \varphi)$, illustrating twisted magnetic field lines and the concept of flux surfaces. Observe that the twist has been exaggerated and in reality there is typically less than one poloidal turn per toroidal turn.

To describe a magnetic equilibrium one introduces toroidal/poloidal coordinates $(r, \theta, \varphi)$, where the physical quantities are $2\pi$-periodic in the toroidal angle $\varphi$ and poloidal angle $\theta$ for fixed $r$. The long way around the torus is the toroidal direction and the short way is the poloidal direction. The flux surfaces are normally not circular over a cross section and it is customary to use a quantity which is constant on flux surfaces, a *flux function*, as a radial coordinate (instead of $r$). A common choice is the poloidal magnetic flux between the surface and the magnetic axis divided by $2\pi$, $\psi = \Psi_p/2\pi$, but another convenient choice is the toroidal flux $\chi_t = \Psi_T/2\pi$. Considering an infinitesimal annulus between two flux surfaces separated by $dr$, as illustrated in Fig. 2.2, the differential poloidal flux is written $d\Psi_p = 2\pi R B_\theta dr$ [8]. Both $\psi$ and $\chi_t$ are radially

monotonically increasing and can be written as functions of each other. Moreover, it can be shown that a possible vector potential associated with the magnetic field of a toroidal fusion device, i.e. $\mathbf{B} = \nabla \times \mathbf{A}$, is $\mathbf{A} = \chi_t \nabla\theta - \psi\nabla\varphi$ [9].

In transport calculations it is common to calculate quantities in terms of their flux surface averages. The flux surface average of a quantity $\mathcal{Q}$, denoted by $\langle\mathcal{Q}\rangle$, is defined as the volume average of $\mathcal{Q}$ between two neighboring flux surfaces $\psi$ and $\psi + d\psi$ [7],

$$\langle\mathcal{Q}\rangle(\psi) \equiv \int \mathcal{Q}\, dV \Big/ \int dV, \tag{2.4}$$

with $dV = g^{1/2} d\psi\, d\theta\, d\varphi$ where $g^{1/2} = 1/\left|(\nabla\varphi \times \nabla\psi)\cdot\nabla\theta\right|$ is the Jacobian.

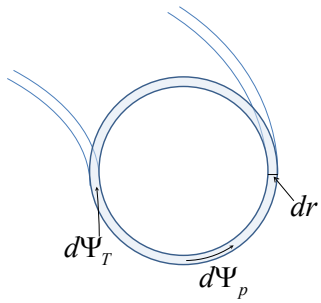


**Figure 2.2:** Flux annulus of width $dr$ containing the poloidal flux $d\Psi_p$ and toroidal flux $d\Psi_T$ (adapted from [8]).

Most magnetic fusion devices have a twisted magnetic field, i.e. both a toroidal $B_\varphi$ and a poloidal $B_\theta$ component, in order to cancel out the particle drifts described by Eq. (2.2) on a particle orbit average. A purely toroidal field would result in charge separation through the magnetic drifts. This would then lead to a rising electric field and thus to severe radial losses by the $\mathbf{E} \times \mathbf{B}$ drift. Because of the twist, particles spend half of their time drifting away from a given radial location, and half of their time approaching it. There are three ways of generating a twisted toroidal magnetic field: driving a toroidal current in the plasma; elongating the flux surfaces and making them rotate poloidally when moving along the torus; or using a non-planar magnetic axis [10]. The method used differs between different types of devices, and the two most common types of experimental devices are the tokamak and the stellarator.

### 2.3.1 Tokamaks

The tokamak is an axisymmetric magnetic fusion device which uses coils to generate the toroidal magnetic field, and drives a toroidal current in the plasma to generate the poloidal magnetic field (in reality a tokamak is not fully axisymmetric, because of the finite number of toroidal field coils a magnetic ripple appears). In an axisymmetric device with circular unshifted cross section (which is usually not valid in real experiments but often used as an approximation in theory) it is possible to choose the toroidal/poloidal coordinates such that they relate to Cartesian coordinates $(\mathrm{x}, \mathrm{y}, \mathrm{z})$ by

$$\begin{aligned} \mathrm{x} &= (R_0 + r\cos\theta)\cos\varphi \\ \mathrm{y} &= (R_0 + r\cos\theta)\sin\varphi \\ \mathrm{z} &= r\sin\theta. \end{aligned} \tag{2.5}$$

$R_0$ and $r$ denote the major and minor radii, and $r = a$ at the edge of the device. The parameters are illustrated in Fig. 2.1 (note that $(r, \theta, \varphi)$ here is a left-handed coordinate system). The ratio $R_0/r$ is normally referred to as the aspect ratio while $\epsilon = r/R_0$ is the inverse aspect ratio. In theoretical work it is common to analyze the large-aspect-ratio limit ($\epsilon \ll 1$).

In tokamaks, an important flux surface parameter is the *safety factor*, $q(\psi) = d\chi_t(\psi)/d\psi$, which is a measure of the helical "twistedness" of the field lines. The safety factor is dimensionless and tells how many toroidal turns are required to encircle the flux surface once poloidally, when following a magnetic field line. In the large-aspect-ratio limit the safety factor can be approximated as $q \approx (rB_\varphi)/(R_0 B_\theta)$. To avoid major instabilities the safety factor should be kept above one everywhere in a tokamak, which means that the toroidal magnetic field component has to be significantly larger than the poloidal component. Another important parameter is the magnetic shear, $s = r\,d(\ln q)/dr$, saying how $q$ changes radially when changing flux surface. In tokamaks $s$ is usually positive implying that $q$ increases monotonically from the center to the edge, however there are scenarios where a negative $s$ can be beneficial.

A common geometry to analyze theoretically (which we employ in this thesis) is the large-aspect-ratio limit with circular cross section and small plasma pressure compared to the magnetic field pressure ($\beta \equiv 2\mu_0 p/B^2 \ll 1$). Then the equilibrium is very simple and the magnetic field strength is given by $B = B_0/(1 + \epsilon\cos\theta)$, with $B_0$ being the field strength on the magnetic axis. Most tokamaks however are non-circular

and $\beta$ can be a few percent. For shaped equilibria and high $\beta$ one must solve the *Grad-Shafranov equation* [8] to find the equilibrium, codes simulating tokamak transport usually have a model to parameterize the plasma in this equilibrium.

### 2.3.2 Stellarators

A stellarator generates its magnetic field from field coils alone. The avoidance of Ohmic current drive has several advantages, such as inherent steady state operation and a small likelihood of inducing major disruptions. On the other hand the stellarator is an inherently 3D magnetic configuration. In a non-axisymmetric plasma flux surfaces are not mathematically guaranteed to exist throughout the plasma in general [10]. Nevertheless, the most common approach is to assume the existence of nested flux surfaces when computing the magnetic equilibrium. A stellarator flux surface is illustrated in Fig. 2.3.

In stellarator research it is customary to talk about the *rotational transform* $\iota$ rather than the safety factor when describing the helical "twistedness" of the field lines, but the two are simply related by $\iota = d\psi/d\chi_t = 1/q$. In a stellarator $\iota$ increases with the minor radius of the device, whereas in a tokamak it decreases. This means that the two different devices have opposite sign of the global magnetic shear. A useful set of magnetic coordinates which is commonly used for stellarators are the Boozer coordinates [11], in which the magnetic field can be written as

$$\mathbf{B} = I\left(\chi_t\right)\nabla\theta + G\left(\chi_t\right)\nabla\varphi + K\left(\chi_t, \theta, \varphi\right)\nabla\chi_t. \tag{2.6}$$

The flux functions $I\left(\chi_t\right)$ and $G\left(\chi_t\right)$ have the simple physical interpretation of being the toroidal current inside and the poloidal current outside the flux surface $\chi_t$ (multiplied by the factor $\mu_0/2\pi$) respectively. Since in a stellarator there is no Ohmic current, typically $|I| \ll |G|$ and $G \approx B_0 R$ where $B_0$ here is the $(0,0)$ Fourier mode amplitude of the magnetic field.

### 2.3.3 Particle trapping and bootstrap current

The magnetic field strength of a tokamak is inversely proportional to $R$, i.e. $B \propto 1/R$. As a consequence of this, the mirror force described earlier gives rise to the phenomenon of *trapped particles*. The trapped particles are particles with so high magnetic moment compared to their kinetic energy, that they are not able to make a complete poloidal turn before they are reflected back by the mirror force. They are therefore trapped

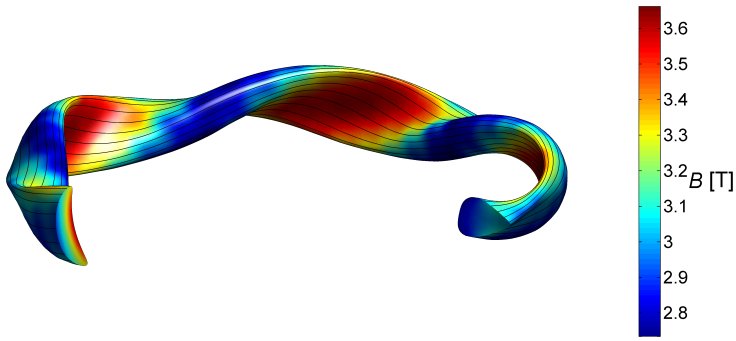


**Figure 2.3:** A stellarator flux surface with its magnetic field lines. The color map represents the strength of the magnetic field.

on the low-field-side in a tokamak, which implies that they bounce back and forth on the outboard side of the torus. The poloidal projections of their guiding center trajectories have banana shapes and are commonly referred to as *banana orbits* [7]. The phenomenon is illustrated in Fig. 2.4. The trapped particles constitute a fraction $\sim \sqrt{\epsilon}$ of the total number of particles and can be responsible for a major part of the radial transport.

Because of the complex shape of the magnetic field in a stellarator, particles are not only trapped in banana orbits on the outboard side of the torus. They can also be trapped in the local magnetic mirrors of the helical field. These helically trapped particles bounce back and forth in a small poloidal range, and can drift outwards and escape the plasma even in the absence of collisions.

A consequence of the trapped particle orbits is the bootstrap current. Because of the pressure gradient there is a net flow of trapped particles in one direction of an intersection between two neighboring bounce orbits, leading to a plasma current parallel to the magnetic field. The current is amplified by the friction which the circulating particles experience on the trapped particles, and it is hence carried by both trapped and passing particles. The bootstrap current is important for tokamaks since it can constitute a substantial fraction of the total plasma current and thus improve confinement. However, in a stellarator the bootstrap current modifies the externally applied magnetic field and it is therefore often desirable to minimize it by an optimization procedure.

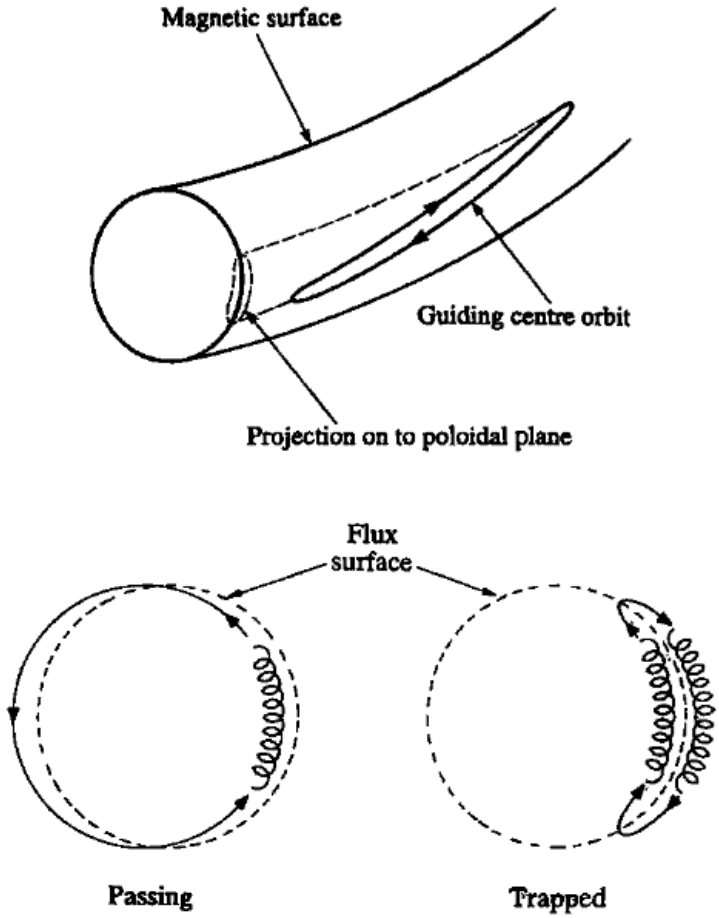


**Figure 2.4:** The upper figure shows the banana orbit of a trapped particle, illustrating how it bounces back and forth on the low-field-side of the tokamak. The lower figure shows the poloidal projection for the orbit of a passing particle (left) and trapped particle (right) (figures from [8]).

## 2.4 Fluid drifts

The drifts described by Eq. (2.2) apply to single charged particles in a strong magnetic field. Often it is useful to describe a fusion plasma through a statistical approach or as a fluid, rather than a collection of discrete particles. It is then possible to see that another macroscopic drift arises, which is present even in the absence of single particle guiding center drifts. This drift is called the *diamagnetic drift* and is due to the inevitable pressure gradient (i.e. gradient of density and/or temperature) present in magnetic fusion plasmas. The name of the drift stems from the fact that plasmas are naturally diamagnetic, i.e. the gyro orbits of the charged particles produce small magnetic fields being in the opposite direction to the total magnetic field [8]. The drift can be understood from the simple picture in Fig. 2.5 [1]. If the plasma density is larger at the top than at the bottom, there are more ions going to the left than to the right. Similarly if the plasma temperature is larger at the top, the ions going to the left have larger velocity on average than the ions going to the right. The ion fluid in a small volume element consequently has an average flow towards left. This is the ion diamagnetic drift, denoted by $v_{*i}$. The electron diamagnetic drift $v_{*e}$ is in the opposite direction, due to the negative charge and the corresponding reversed direction of the electron gyration. The diamagnetic flows result in a diamagnetic current perpendicular to the magnetic field, which in general is not divergence free. However, the total current must be divergence free to ensure quasi-neutrality and consequently a parallel current must exist to fulfill this requirement. This leads to the *Pfirsch-Schlüter* current driven by the pressure gradient.

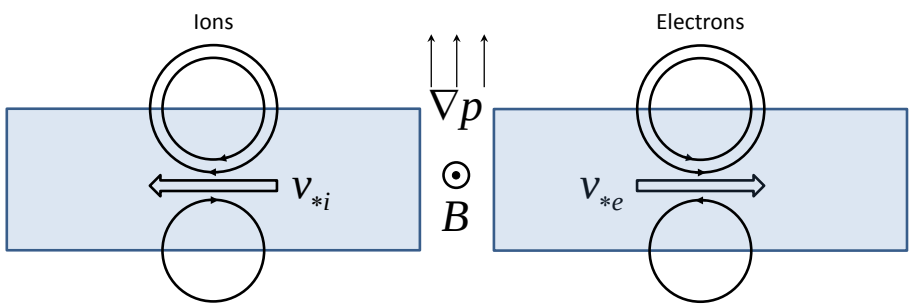


**Figure 2.5:** Illustration of how the diamagnetic drift arises (adapted from [1]). Note that the electron gyro orbit has been exaggerated, as compared to the ion orbit.

# Chapter 3

# Kinetic transport theory

## 3.1 Transport theory

A major part of the theoretical work for toroidal magnetized fusion plasmas is directed towards the understanding of the radial transport of particles and energy. To maximize the energy confinement time, one should search for configurations where the outward radial transport of electrons and main ions is minimized. At the same time it is desirable to have transport of impurities out of the core to the edge of a plasma. The most obvious way that the transport occurs in a fusion plasma is through the Coulomb interaction between the charged plasma particles, referred to as collisional or classical transport (when the effects of the geometry are taken into account one often speaks of neoclassical transport). However, today there is a consensus that the collisional transport is in many situations overshadowed by transport caused by small scale collective instabilities, typically driven by the gradients of density and temperature. A main objective of transport theory is consequently to understand and predict the numerous different instabilities that can arise in a fusion plasma. Large scale MHD instabilities can also occur, sometimes leading to disruptions which can cause termination of a tokamak plasma and should therefore be avoided. These instabilities can be prevented by operating the plasma in the right regimes.

Since a fusion plasma is a collection of $\sim 10^{20}$ charged particles in constant motion it is not possible to follow the evolution of each individual particle in a tractable way. The most sophisticated existing description is the kinetic theory which describes each plasma species $\alpha$ through its phase space distribution function $f_\alpha(t, \mathbf{r}, \mathbf{v})$, where $t$ is time, $\mathbf{r}$ position

and $\mathbf{v}$ velocity. From the distribution function, macroscopic quantities such as densities, fluxes, flows and currents, can be determined by taking appropriate moments and averages. In a plasma the particles move according to the equations of motion

$$\begin{aligned} \frac{d\mathbf{r}}{dt} &= \mathbf{v} \\ \frac{d\mathbf{v}}{dt} &= \frac{e_\alpha}{m_\alpha}\left(\mathbf{E} + \mathbf{v} \times \mathbf{B}\right), \end{aligned} \tag{3.1}$$

where $e_\alpha \left(\mathbf{E} + \mathbf{v} \times \mathbf{B}\right)/m_\alpha$ is the acceleration due to the Lorentz force. Defining the 6-dimensional phase space as $\mathbf{z} = (\mathbf{r}, \mathbf{v})$, the evolution of the distribution function is determined from the *Fokker-Planck equation* [7, 8]

$$\begin{aligned} \frac{df_\alpha}{dt} &\equiv \frac{\partial f_\alpha}{\partial t} + \frac{\partial}{\partial \mathbf{z}} \cdot \left(\frac{d\mathbf{z}}{dt} f_\alpha\right) = \\ &= \left(\frac{\partial f_\alpha}{\partial t}\right)_{\mathbf{v}} + \mathbf{v} \cdot \left(\nabla f_\alpha\right)_{\mathbf{v}} + \frac{e_\alpha}{m_\alpha}\left(\mathbf{E} + \mathbf{v} \times \mathbf{B}\right) \cdot \nabla_v f_\alpha = C_\alpha\left[f_\alpha\right]. \end{aligned} \tag{3.2}$$

Subscripts on partial derivatives indicate quantities that are held fixed in the differentiation. $C_\alpha\left[f_\alpha\right] = \sum_b C_{\alpha b}\left[f_\alpha, f_b\right]$ is the *Coulomb collision operator* describing the change in distribution as a result of Coulomb collisions with all plasma species ($C_{\alpha b}\left[f_\alpha, f_b\right]$ describes collisions of species $\alpha$ on species $b$). $\mathbf{E}$ and $\mathbf{B}$ represent the macroscopic electric and magnetic fields. The microscopic parts of these fields, which are fluctuating on spatial scales comparable to or smaller than the Debye length, are contained in the collision operator. For discussions on the derivation of the *Fokker-Planck equation*, see e.g. Refs. [12–14]. A plasma is completely described in a self-consistent way by the Fokker-Planck equation for each plasma species coupled with Maxwell's equations. The problem is that this system of equations is highly complex and tedious to treat in reality, and often one resorts to different simplifications.

In collisional transport theory, appropriate for quiescent plasmas, the macroscopic fields in Eq. (3.2) are often not determined self-consistently by coupling to Maxwell's equations [15]. In *classical* theory the fields are simply replaced by given external fields, $\mathbf{E} \approx \mathbf{E}_0$ and $\mathbf{B} \approx \mathbf{B}_0$, where $\mathbf{E}_0$, $\mathbf{B}_0$ are stationary and homogeneous. *Neoclassical* transport theory takes the toroidal magnetic geometry into account, with $\mathbf{B}$ obtained from an equilibrium solution of the macroscopic MHD equations. Common to

these approaches is that the fields are determined independently of the particle distribution functions, and then substituted into Eq. (3.2) as given functions.

In contrast to collisional transport theory, turbulent transport theory (discussed in Sec. 3.3) introduces fluctuating fields into Eq. (3.2) and couples it to Maxwell's equations. For a turbulent plasma, a statistical description is best suited.

### 3.1.1 Fluid approach

As mentioned earlier, macroscopic quantities are obtained by taking velocity moments of $f_\alpha$, i.e. integrating over velocity space: $\int d^3v \equiv \int_{-\infty}^{\infty} dv_\parallel \int_0^\infty dv_\perp\, v_\perp \int_0^{2\pi} d\zeta$, where $\zeta$ is the gyro-phase, i.e. $\mathbf{v} = v_\parallel \mathbf{b} + v_\perp \left[\mathbf{e}_1 \cos\zeta + \mathbf{e}_2 \sin\zeta\right]$ such that $(\mathbf{e}_1, \mathbf{e}_2, \mathbf{b})$ forms a right handed orthonormal basis. For example, the particle density is obtained as the $0^{\text{th}}$ moment, $n_\alpha(t,\mathbf{r}) = \int f_\alpha(t,\mathbf{r},\mathbf{v})\, d^3v$. It is convenient to denote the average of a quantity $A$ over the particle distribution by $\langle A\rangle_f \equiv \int A f_\alpha d^3v / n_\alpha$. Now the local particle temperature can be defined as $T_\alpha(t,\mathbf{r}) \equiv \left\langle m_\alpha (\mathbf{v}-\mathbf{V}_\alpha)^2 \right\rangle_f /3$, where $\mathbf{V}_\alpha(t,\mathbf{r}) = \langle \mathbf{v}\rangle_f$ is the macroscopic fluid velocity.

One way to proceed from Eq. (3.2) is by forming velocity moments of the equation, and by this approach we obtain fluid equations. The $\left\{1, m\mathbf{v}, mv^2/2\right\}$ velocity moments of Eq. (3.2) describe the conservation properties of particles, momentum and energy [7]

$$\frac{\partial n_\alpha}{\partial t} + \nabla\cdot(n_\alpha \mathbf{V}_\alpha) = 0, \tag{3.3}$$

$$\frac{\partial m_\alpha n_\alpha \mathbf{V}_\alpha}{\partial t} + \nabla\cdot\boldsymbol{\Pi}_\alpha = n_\alpha e_\alpha (\mathbf{E} + \mathbf{V}_\alpha \times \mathbf{B}) + \int d^3v\, C_\alpha[f_\alpha]\, m_\alpha \mathbf{v}, \tag{3.4}$$

$$\frac{\partial}{\partial t}\left(\frac{3 n_\alpha T_\alpha}{2} + \frac{m_\alpha n_\alpha V_\alpha^2}{2}\right) + \nabla\cdot\mathbf{Q}_\alpha = n_\alpha e_\alpha \mathbf{E}\cdot\mathbf{V}_\alpha + \int d^3v\, C_\alpha[f_\alpha]\, \frac{m_\alpha v^2}{2}. \tag{3.5}$$

Here we have introduced the momentum flux tensor $(\boldsymbol{\Pi}_\alpha)_{jk} \equiv \langle m_\alpha n_\alpha v_j v_k\rangle_f$ and the energy flux $\mathbf{Q}_\alpha \equiv m_\alpha n_\alpha \langle v^2 \mathbf{v}\rangle_f /2$. The last terms of Eq. (3.4) and Eq. (3.5) can be rewritten by introducing the friction force $\mathbf{R}_\alpha \equiv \int d^3v C_\alpha[f_\alpha]\, m_\alpha \mathbf{v}$ and the rate of thermal energy transfer $\mathcal{Q}_\alpha \equiv \int d^3v C_\alpha[f_\alpha]\, m_\alpha |\mathbf{v}-\mathbf{V}_\alpha|^2/2 = \int d^3v C_\alpha[f_\alpha]\, m_\alpha v^2/2 - \mathbf{R}_\alpha\cdot\mathbf{V}_\alpha$,

consequently these quantities describe the Coulomb interaction with other species.

One important objective of transport theory is to determine the space-time evolution of $n_\alpha$, $\mathbf{V}_\alpha$ and $T_\alpha$ for all plasma species. To perform simulations based on the fluid equations is a widespread approach, but the major issue is that each moment equation couples to one higher up in the hierarchy. This means that we would need to take an infinite number of moments to obtain a closed system of equations. Instead one must introduce approximations to obtain closure. A kinetic approach is more sophisticated, but at the same time more expensive to use. One of the historically most famous ways to close the fluid equations was introduced by Braginskii in 1965 [16]. The equations are applicable to a single-ion species plasma in the short mean-free-path limit (i.e. high collisionality), assuming $\partial/\partial t \ll \nu_\alpha$ and $v_{th,\alpha}/\nu_\alpha \ll L$ with $v_{th,\alpha} = \sqrt{2T_\alpha/m_\alpha}$ being the thermal velocity and $L$ the length scale of variation of macroscopic plasma parameters. However, today there exist fluid approaches which are more appropriate in a hot core plasma.

### 3.1.2 Drift-kinetic and gyrokinetic approaches

To describe transport processes in fusion plasmas, it is usually not necessary to resolve time scales comparable to or faster than the rapid ion gyro motion. By making use of the smallness of the Larmor radius as compared to the typical length scales, a gyro-phase averaging can be performed on the kinetic equation. This implies that we only follow the distribution of particle guiding centers and ignore the gyro-phase, thus reducing the description from 6D phase-space to 5 dimensions. In collisional transport theory in toroidally symmetric fields the so called drift-kinetic equation is mainly used, representing particles as drifting guiding centers with a charge and magnetic dipole moment. An extended introduction to collisional transport through the drift-kinetic approach is presented in Section 3.2. For turbulent transport, which we will treat in Section 3.3, the gyrokinetic equation is more suitable because it allows for sharp spatial variations in the perturbed fields and in the distributions on scales as small as the electron Larmor radius.

### 3.1.3 Fluxes

The different fluxes in a plasma are produced by the thermodynamic forces, related to the spatial inhomogeneities such as the density and

temperature gradients, $\nabla n_\alpha$ and $\nabla T_\alpha$. As an example, from a simple random walk estimate we can derive Fick's law [7, 15] relating the local diffusive collisional particle flux to the density gradient

$$\mathbf{\Gamma}_\alpha = -D_\alpha \nabla n_\alpha, \tag{3.6}$$

and Fourier's law relating the local heat flux to the temperature gradient

$$\mathbf{q}_\alpha = -n_\alpha \chi_\alpha \nabla T_\alpha. \tag{3.7}$$

Here $D_\alpha$ is called the diffusion coefficient and $\chi_\alpha$ the heat diffusivity.

The most important transport quantities for a magnetic fusion plasma are the flux surface average of the cross-field particle and energy fluxes which we denote by $\Gamma_{\alpha\perp}$ and $Q_{\alpha\perp}$ respectively. If we know the species distribution function they can readily be calculated as

$$\Gamma_{\alpha\perp} \equiv \langle \mathbf{\Gamma}_\alpha \cdot \nabla r \rangle = \left\langle \int d^3v f_\alpha \mathbf{v} \cdot \nabla r \right\rangle \tag{3.8}$$

and

$$Q_{\alpha\perp} \equiv \langle \mathbf{Q}_\alpha \cdot \nabla r \rangle = \left\langle \int d^3v \frac{m_\alpha v^2}{2} f_\alpha \mathbf{v} \cdot \nabla r \right\rangle. \tag{3.9}$$

The cross-field particle flux is sometimes divided into separate contributions as,

$$\Gamma_{\alpha\perp} = -D_\alpha \frac{dn_\alpha}{dr} - H_\alpha \frac{dT_\alpha}{dr} - n_\alpha V_\alpha. \tag{3.10}$$

The three terms on the right hand side of Eq. (3.10) represent diffusion, thermodiffusion and convective flux ("pinch flux") respectively. The coefficients $D_\alpha$, $H_\alpha$ and $V_\alpha$ depend on the plasma parameters.

## 3.2 Collisional transport

The basis for all calculations of cross-field neoclassical transport and flows, as well as the bootstrap current, is the drift-kinetic equation. The theory is based on expanding the kinetic equation (Eq. (3.2)) in the smallness of the Larmor radius as compared to the typical length scales of interest, and performing a gyro-phase averaging.

### 3.2.1 Derivation of the drift-kinetic equation

A derivation of the equation is presented in [17], and here we outline some of the main features. The drift-kinetic equation is derived from the Fokker-Planck equation (Eq. (3.2)) by expanding the equation in the small parameter $\rho_* = \rho_\alpha / L \ll 1$, where $\rho_\alpha = v_{th,\alpha}/\Omega_\alpha$ is the thermal Larmor radius and $L$ is a typical length scale for variation of macroscopic quantities ($\mathbf{B}$, $f$, $\phi$), e.g. $L \approx a$ the plasma minor radius. Expanding the distribution function as $f_\alpha = f_{\alpha 0} + f_{\alpha 1} + \ldots$, the following ordering is employed

$$\frac{f_{\alpha\,(j+1)}}{f_{\alpha j}} \sim \frac{\nu_\alpha}{\Omega_\alpha} \sim \frac{|\mathbf{v}_E|}{v_{th,\alpha}} \sim \rho_*, \tag{3.11}$$

where $\mathbf{v}_E$ is the $\mathbf{E}\times\mathbf{B}$ drift part of Eq. (2.2) (note that $\nu_\alpha/\Omega_\alpha \ll 1$ is practically always satisfied with a wide margin, since otherwise the magnetic fields would be too weak to confine the plasma). The ordering of $\mathbf{v}_E$ here is the low-flow ordering, but there are approaches which allow for larger flows. Furthermore the electric field is assumed to be electrostatic to leading order $\mathbf{E}_0 = -\nabla\phi_0$, with $\mathbf{E} - \mathbf{E}_0 \equiv \mathbf{E}_1 \sim \rho_* \mathbf{E}$, and time derivatives are taken to be small $\partial/\partial t \sim \rho_*^2 \Omega_\alpha$. It is convenient to derive the drift-kinetic equation using guiding center coordinates $(\mathbf{R}, \mathcal{W}, \mathcal{U}, \zeta)$, where $\mathcal{W} = v^2/2 + e_\alpha \phi_0 / m_\alpha$ and $\mathcal{U} = v_\perp^2/(2B)$, i.e. the energy and magnetic moment normalized to the species mass $m_\alpha$. Equation (3.2) is then rewritten as

$$\frac{\partial f_\alpha}{\partial t} + \mathbf{v}\cdot\nabla f_\alpha + \frac{d\mathcal{W}}{dt}\frac{\partial f_\alpha}{\partial \mathcal{W}} + \frac{d\mathcal{U}}{dt}\frac{\partial f_\alpha}{\partial \mathcal{U}} + \frac{d\zeta}{dt}\frac{\partial f_\alpha}{\partial \zeta} = C_\alpha\left[f_\alpha\right]. \tag{3.12}$$

We now introduce the gyro-phase average for any quantity $G(\mathbf{R},\zeta)$ defined as $\overline{G} \equiv \langle G(\mathbf{R},\zeta)\rangle_{\mathbf{R}} \equiv (2\pi)^{-1}\int_0^{2\pi} d\zeta G(\mathbf{R},\zeta)$, where position, $\mathcal{W}$ and $\mathcal{U}$ are kept fixed in the integration. It is possible to show that $d\mathcal{W}/dt = e_\alpha \mathbf{E}_1\cdot\mathbf{v}/m_\alpha$, $\overline{d\mathcal{W}/dt} = e_\alpha E_{1\parallel} v_\parallel / m_\alpha$, $d\mathcal{U}/dt = -\mathcal{U}\mathbf{v}\cdot\nabla B/B - v_\parallel \mathbf{v}\mathbf{v} : (\nabla\mathbf{b})/B + e_\alpha \mathbf{E}\cdot\mathbf{v}_\perp/m_\alpha B$[1], $\overline{d\mathcal{U}/dt} = 0$, and that $d\zeta/dt = -\Omega_\alpha + \mathcal{G}$ where $\mathcal{G}$ only consists of terms of order $\rho_*\Omega_\alpha$ or smaller. By introducing $\breve{f}_\alpha = f_\alpha - \overline{f_\alpha}$, we can rewrite Eq. (3.12) as

$$\frac{\partial \overline{f_\alpha}}{\partial t} + \mathbf{v}\cdot\nabla\overline{f_\alpha} + \frac{d\mathcal{W}}{dt}\frac{\partial \overline{f_\alpha}}{\partial \mathcal{W}} + \frac{d\mathcal{U}}{dt}\frac{\partial \overline{f_\alpha}}{\partial \mathcal{U}} + \frac{d\breve{f}_\alpha}{dt} = C_\alpha\left[\overline{f_\alpha} + \breve{f}_\alpha\right]. \tag{3.13}$$

Applying the gyro-average to Eq. (3.13) yields

$$\frac{\partial \overline{f_\alpha}}{\partial t} + v_\parallel \mathbf{b}\cdot\nabla\overline{f_\alpha} + \frac{e_\alpha}{m_\alpha} E_{1\parallel} v_\parallel \frac{\partial \overline{f_\alpha}}{\partial \mathcal{W}} + \overline{\frac{d\breve{f}_\alpha}{dt}} = \overline{C_\alpha\left[\overline{f_\alpha} + \breve{f}_\alpha\right]}, \tag{3.14}$$

[1] The operator : is the double-dot product between dyadics.

and subtracting Eq. (3.14) from Eq. (3.13) we obtain

$$\mathbf{v}_\perp \cdot \nabla \overline{f_\alpha} + e_\alpha \mathbf{E}_{1\perp} \cdot \mathbf{v}_\perp \frac{\partial \overline{f_\alpha}}{\partial \mathcal{W}} + \frac{d\mathcal{U}}{dt} \frac{\partial \overline{f_\alpha}}{\partial \mathcal{U}} + \frac{d\breve{f}_\alpha}{dt} - \overline{\frac{d\breve{f}_\alpha}{dt}} = \\ = C_\alpha \left[ \breve{f}_\alpha + \overline{f_\alpha} \right] - \overline{C_\alpha \left[ \breve{f}_\alpha + \overline{f_\alpha} \right]}. \quad (3.15)$$

Now applying the orderings in Eq. (3.11), the leading order term in Eq. (3.12) gives $-\Omega_\alpha \partial f_{\alpha 0}/\partial \zeta = 0$ which means that $\breve{f}_{\alpha 0} = 0$, so $f_{\alpha 0} = \overline{f_{\alpha 0}}$ and $\breve{f}_\alpha \sim \rho_* \overline{f_\alpha}$. Next, the leading terms in Eq. (3.14) of order $\mathcal{O}\left(\rho_* \Omega_\alpha \overline{f}_\alpha\right)$ yields

$$v_\parallel \mathbf{b} \cdot \nabla f_{\alpha 0} = \overline{C_\alpha \left[ f_{\alpha 0} \right]}, \quad (3.16)$$

and it can be shown (see e.g. Ref. [7]) that the solution must be a Maxwellian,

$$f_{\alpha 0} = \frac{N_\alpha(\psi)}{(2\pi T_\alpha/m_\alpha)^{3/2}} \exp\left( -\frac{m_\alpha (\mathbf{v} - \mathbf{V}_{\alpha 0})^2}{2T_\alpha} - \frac{e_\alpha \phi}{T_\alpha} \right), \quad (3.17)$$

where $N_\alpha(\psi) = n_\alpha(\psi, \theta, \varphi) \exp\left(\frac{e_\alpha \phi}{T_\alpha}\right)$ is the pseudo-density ($n_\alpha(\psi, \theta, \varphi)$ is the density) and with the property $C_\alpha[f_{\alpha 0}] = 0$. We note that the variation of the electrostatic potential on a flux surface is often weak in tokamaks, i.e. $e_\alpha(\phi - \langle\phi\rangle)/T_\alpha \sim \rho_* \ll 1$, implying that the density is a flux function $n_\alpha(\psi, \theta, \varphi) = n_\alpha(\psi)$. However there are situations, for both tokamak and stellarator plasmas, where the variation is large enough to affect ion species of high charge $e_\alpha = Ze \gg e$ and should be taken into account. Such situations are analyzed for tokamaks in this thesis.

To continue the derivation we will replace the collision operator by the linearized collision operator $C_\alpha[f_\alpha] \simeq C_\alpha^{(l)}[f_\alpha]$ and use the approximation $\overline{C_\alpha^{(l)}[f_\alpha]} \simeq C_\alpha^{(l)}\left[\overline{f_\alpha}\right]$ (collision operators are discussed in Section 3.2.2). From the $\mathcal{O}(\rho_* \Omega_\alpha f_{\alpha 0})$ terms of Eq. (3.15) we obtain

$$\mathbf{v}_\perp \cdot \nabla f_{\alpha 0} - \Omega_\alpha \frac{\partial \breve{f}_{\alpha 1}}{\partial \zeta} = 0, \quad (3.18)$$

which may be integrated to give

$$\breve{f}_{\alpha 1} = -\left(\Omega_\alpha^{-1} \mathbf{b} \times \mathbf{v}\right) \cdot \nabla f_{\alpha 0} \quad (3.19)$$

since $\mathbf{v}_\perp = \partial(\mathbf{v}\times\mathbf{b})/\partial\zeta$. The drift-kinetic equation, for the gyro-averaged distribution $\overline{f_{\alpha 1}}$, is obtained from the $\mathcal{O}\left(\rho_*^2\Omega_\alpha f_{\alpha 0}\right)$ terms of Eq. (3.14)

$$v_\parallel \mathbf{b}\cdot\nabla\overline{f_{\alpha 1}} - \frac{e_\alpha}{T_\alpha}E_{1\parallel}v_\parallel f_{\alpha 0} + \overline{\frac{d\breve{f}_{\alpha 1}}{dt}} = C_\alpha^{(l)}\left[\overline{f_{\alpha 1}}\right]. \tag{3.20}$$

Using Eq. (3.19) the $\overline{d\breve{f}_{\alpha 1}/dt}$ term can be calculated, and since $E_\parallel = \mathbf{b}\cdot\mathbf{E} = \mathbf{b}\cdot(\mathbf{E}_1 - \nabla\phi_0) = \mathbf{b}\cdot\mathbf{E}_1 = E_{1\parallel}$, Eq. (3.20) can finally be rewritten as

$$v_\parallel \mathbf{b}\cdot\nabla\overline{f_{\alpha 1}} + \mathbf{v}_d\cdot\nabla f_{\alpha 0} + \frac{e_\alpha}{m_\alpha}E_\parallel v_\parallel\frac{\partial f_{\alpha 0}}{\partial\mathcal{W}} = C_\alpha^{(l)}\left[\overline{f_{\alpha 1}}\right], \tag{3.21}$$

where the drift velocity $\mathbf{v}_d$ is defined in Eq. (2.2) (in $\mathbf{v}_d$ we have neglected the parallel velocity correction as it is small compared to the parallel streaming term $v_\parallel\mathbf{b}\cdot\nabla\overline{f_{\alpha 1}}$). $\mathbf{v}_d\cdot\nabla f_{\alpha 0} = (\mathbf{v}_d\cdot\nabla\psi)\,\partial f_{\alpha 0}/\partial\psi$ represents the effect of the cross-field drift. One of the main objectives of neoclassical theory is to solve Eq. (3.21) in various collisionality regimes.

### 3.2.2 Collisions

In a quiescent plasma, without turbulence, the cross-field particle and energy transport is completely determined by collisional processes. Furthermore collisions play an important role in turbulent transport as well. How accurate the model of the collision operator is, consequently affects how well the transport processes in the plasma can be predicted. Due to the long range nature of the Coulomb interaction, and that the number of particles within a Debye sphere of a plasma is large, each particle is constantly interacting with a large number of other particles. Small angle-scattering dominates over large deflections, and a single particle follows a smooth trajectory. The collision operator $C_\alpha[f_\alpha] = \sum_b C_{\alpha b}[f_\alpha, f_b]$ describes the change in the distribution $f_\alpha$ of species $\alpha$ due to interaction with all plasma species $b$, and is truly complicated to treat. A realistic collision operator should conserve particles, momentum and energy, and in its most sophisticated form $C_{\alpha b}$ is given by the Fokker-Planck collision operator (see e.g. Eq. (3.21) of Ref. [7]). In practice, due to its complexity, this form is often still intractable to use, even with the best simulation tools available, and one has to resort to simplifications. Approximations can be made in special cases, such as when the colliding species have significantly different masses, or for a species colliding with

a Maxwellian background, but these approximations can also be difficult to implement. One crucial property of a useful collision operator is that it should drive the system towards local thermodynamic equilibrium. Importantly for two Maxwellian distributions $f_{M\alpha}$, $f_{Mb}$ with equal temperatures and mean velocities, the collision operator should vanish, $C_{\alpha b}\left[f_{M\alpha}, f_{Mb}\right] = C_{b\alpha}\left[f_{Mb}, f_{M\alpha}\right] = 0$.

Due to the smoothness of Coulomb collisions, it is common to define the collision time $\tau$ as the time required for an order unity relative change in velocity of a particle as a result of the cumulative interaction with other particles. The collision frequency is then defined as $\nu = \tau^{-1}$. The electron-ion collision frequency can be shown to be [7]

$$\nu_{ei} \propto \frac{e^4 n_i Z_i^2 \ln\Lambda}{\epsilon_0^2 m_e^{1/2} T_e^{3/2}}, \tag{3.22}$$

where $\epsilon_0$ is the electric permittivity of free space and $\ln\Lambda$ the Coulomb logarithm (typically $\ln\Lambda \sim 10 - 20$ in a fusion plasma). Furthermore, assuming $T_i \sim T_e$, it can be shown that $\nu_{ei} \sim \nu_{ii}\sqrt{m_i/m_e}/Z_i^2 \sim \nu_{ie} m_i/m_e$ and $\nu_{ee} \sim \nu_{ei}$. It is common to make the following definitions of basic collision frequency and time for species $\alpha$ colliding on species $b$,

$$\hat{\nu}_{\alpha b} \equiv \frac{n_b e_\alpha^2 e_b^2 \ln\Lambda}{2^{1/2} \cdot 8\pi\epsilon_0^2 m_\alpha^{1/2} T_\alpha^{3/2}}, \quad \tau_{\alpha b} \equiv \frac{3\pi^{1/2}}{4\hat{\nu}_{\alpha b}}. \tag{3.23}$$

Since the collision frequency is inversely proportional to $T^{3/2}$, it seems reasonable to neglect collisions in hot parts of fusion plasmas, such as close to the core, when turbulent transport dominates over collisional transport. However, both simulations and experiments have shown that collisions can affect the turbulent transport significantly [18] and often a model of collisions should be included for completeness. A highly simplified model, with the advantage that it is easy to treat, is the Krook operator $C_\alpha\left[f_\alpha\right] = -\nu\left(f_\alpha - f_{M\alpha}\right)$ which simply drives the distribution towards a Maxwellian $f_{M\alpha}$. Here the collision frequency $\nu$ can include an energy dependence.

A more advanced collision operator is the pitch-angle scattering operator (or Lorentz operator)

$$\mathcal{L}\left[f_\alpha\right] \equiv \frac{1}{2}\frac{\partial}{\partial\xi}\left[\left(1-\xi^2\right)\frac{\partial f_\alpha}{\partial\xi}\right], \tag{3.24}$$

where $\xi = v_\parallel/v$ is the cosine of the pitch-angle. This operator describes diffusion on a surface of constant velocity, thus changing the

direction but not the magnitude of the velocity vector. As an example it is useful for describing electrons colliding with the much heavier ions, $C_{ei}\left[f_e, f_i\right] \approx \nu_{ei}\left(v\right)\mathcal{L}\left[f_e\right]$, but can be the dominant contribution in other cases as well.

Lastly, for a system close to local thermodynamic equilibrium (when the distribution is nearly Maxwellian, $f_\alpha = f_{M\alpha} + f_{\alpha 1}$ with $f_{\alpha 1} \ll f_{M\alpha}$) the linearized collision operator $C^{(l)}_{\alpha\alpha}\left[f_\alpha\right] \equiv C_{\alpha\alpha}\left[f_{\alpha 1}, f_{M\alpha}\right] + C_{\alpha\alpha}\left[f_{M\alpha}, f_{\alpha 1}\right]$ can be useful for describing collisions between particles of the same species. Besides being linear, and conserving particles, momentum and energy, it has the important property of being self-adjoint which means that any two functions $\hat{f}\left(\mathbf{v}\right)$, $\hat{g}\left(\mathbf{v}\right)$ satisfy $\int \hat{g} C^{(l)}_{\alpha\alpha}\left[f_{M\alpha}\hat{f}\right] d^3v = \int \hat{f} C^{(l)}_{\alpha\alpha}\left[f_{M\alpha}\hat{g}\right] d^3v$.

### Collisionality regimes

The physics of collisional transport depends on the relative magnitude of the collision frequency $\nu$ and the transit frequency $\omega_t \equiv v_T/qR$ (this ratio is referred to as collisionality), and it is thus customary to talk about different collisionality regimes. If collisionality is large, the mean-free path is shorter than the parallel distance around a flux surface, $L \sim qR$, and the typical particle orbits of thermal particles are interrupted by collisions before being completed. This regime is called the *Pfirsch-Schlüter* (or high-collisionality) regime, and is defined by the condition

$$\frac{\nu}{\omega_t} \gg 1. \tag{3.25}$$

The opposite, low collisionality regime, is often subdivided into the plateau regime

$$\epsilon^{3/2} \ll \frac{\nu}{\omega_t} \ll 1, \tag{3.26}$$

and the banana regime

$$\frac{\nu}{\omega_t} \ll \epsilon^{3/2}, \tag{3.27}$$

where we recall that $\epsilon$ is the inverse aspect ratio. The motivation for this division is that in the plateau regime circulating particle orbits are usually completed but trapped orbits destroyed by collisions, whereas in the banana regime both types of orbits can be completed. This is understood by comparing the effective collision frequency for trapping/de-trapping, $\nu_{\text{eff}} = \nu/\epsilon$, to the particle bounce frequency $\omega_b \sim \epsilon^{1/2}\omega_t$. We note that

the ordering into different regimes refers to thermal particles rather than individual particles, and that there is no distinct transition between the regimes at realistic aspect ratios.

In a stellarator, particles can become trapped in helical magnetic wells over a small poloidal range with superimposed outward radial drift. Because of this, collisionless orbits are not necessarily confined. A poorly designed stellarator magnetic field can therefore lead to rapid collisional losses of particles, and it is thus a bigger challenge for stellarators to control the neoclassical transport of fuel ions than for a tokamak. The helically trapped particles are responsible for the unfavorable confinement regime at high temperatures, known as the $1/\nu$-regime (see Fig. 3.1). However, if a sufficiently large radial electric field $E_r \propto -d\phi/d\chi_t$ is present, the locally trapped particles can be convected poloidally by the $\mathbf{E} \times \mathbf{B}$ precession drift out of the trapped region, preventing them from drifting all the way out of the plasma. This leads to a collisionality regime of reduced confinement degradation, called the $\sqrt{\nu}$-regime.

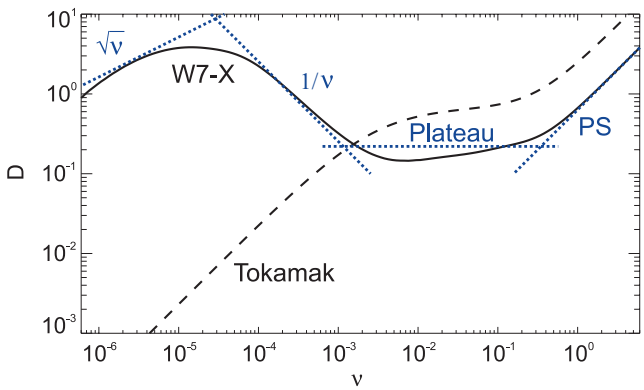


**Figure 3.1:** Comparison of particle diffusion coefficient as function of normalized collision frequency for the W7-X stellarator and a tokamak of similar size. The dotted straight lines show the asymptotic regimes of a stellarator which are (in the order of increasing collisionality): the $\sqrt{\nu}$-regime, the $1/\nu$-regime, the plateau regime and the Pfirsch-Schlüter regime (figure from [10]).

### 3.2.3 Tokamaks vs. Stellarators

It is clear from Fig. 3.1 that at high reactor-like temperatures with a low collisionality, the tokamak has a substantial advantage over the stellarator in terms of a significantly lower collisional transport. In fact, it has

long been known that the collisional transport is usually overshadowed by a much larger turbulent transport in tokamak plasmas. However, in a stellarator the neoclassical transport could be expected to dominate over the turbulent transport in the core because of the $1/\nu$-transport behavior, and sometimes in almost the entire plasma volume [10].

As a consequence of the transport ordering in drift-kinetic theory (Eq. (3.11)), radial neoclassical fluxes in a tokamak are intrinsically ambipolar [7], i.e. the radial current vanishes independently of the radial electric field

$$\sum_{\alpha} e_{\alpha}\Gamma_{\alpha\perp} = 0. \tag{3.28}$$

Because the collisionless trajectories are not necessarily confined this is not the case in a stellarator, where the diffusion coefficient is typically much larger for ions than for electrons (note that the radial turbulent fluxes are automatically ambipolar to leading order in $\rho_*$ for both a tokamak and a stellarator). In response, a radial electric field arises to reduce the ion particle transport down to the electron level. This field is referred to as the ambipolar radial electric field. In the usual situation the ambipolar electric field points inwards, $E_r < 0$, which is known as the "ion root". However, under certain circumstances, such as in the case of strong localized electron heating, $E_r$ can become positive which accordingly is referred to as the "electron root". $E_r$ enters as a thermodynamic force in a stellarator plasma, whereas in a tokamak a radial electric field essentially only causes toroidal rotation of the plasma. The possible level of plasma rotation is another important difference between the axisymmetric tokamak and the non-axisymmetric stellarator. It follows from the drift-kinetic equation (Eq. (3.21)) that fast rotation, of the order of the ion thermal speed $v_{th,i}$, is generally impossible in a stellarator. Plasma rotation on the diamagnetic level, $V \sim \rho_* v_{Ti}$, is set by the ambipolarity requirement. In a tokamak the plasma is essentially free to rotate at any speed. The rotation is determined by the radial transport of angular momentum, the sources (neutral beam injection) and the sinks (friction against neutral particles).

To reduce the large neoclassical transport in 3D plasmas, it is desirable to design devices according to the quasi-symmetric condition. A mathematical definition of quasi-symmetry is that it should be possible to express the magnetic field $B(\psi, \theta, \varphi) = |\mathbf{B}|$ as a function of $\psi$ and $m\theta - n\varphi$, where $m$ and $n$ are integers, and $(\theta, \varphi)$ are the Boozer angles in Eq. (2.6). If this condition is fulfilled, nearly all differences between stellarators and tokamaks concerning collisional transport dis-

appear, i.e. no regimes of $1/\nu$- or $\sqrt{\nu}$-transport appear, and radial fluxes are intrinsically ambipolar. However, exact quasi-symmetry is not possible in practice (except for the $n = 0$ tokamak geometry) and even a small violation can lead to significantly enhanced transport.

### 3.2.4 SFINCS

The Stellarator Fokker-Planck Iterative Neoclassical Conservative Solver [19] is a continuum code, which solves the radially local 4D drift-kinetic equation (Eq. (3.21)) retaining coupling in four of the independent phase space variables (two spatial and two velocity). The complexity due to the extra dimension in 3D devices compared to axisymmetric devices, means that neoclassical calculations have predominantly been performed using simplifying approximations. As an example, including the $\mathbf{E} \times \mathbf{B}$ precession from a radial electric field is important to capture the $\sqrt{\nu}$-regime, but complicated since $\mathbf{E} \times \mathbf{B}$ precession is formally excluded in the usual drift ordering $|\mathbf{v}_E| \sim \rho_* v_{th,i}$. Moreover, including the precession term in the drift-kinetic equation puts unphysical constraints on the distribution function which appear when $E_r \neq 0$ (see Ref. [19] for details). To overcome these difficulties, a common simplification is to make ad-hoc changes to several terms in the drift-kinetic equation, e.g. replacing $1/B^2$ with $1/\langle B^2 \rangle$ in the $\mathbf{E} \times \mathbf{B}$ drift. Together these changes are referred to as the "monoenergetic" approximation, because derivatives of the distribution function with respect to speed are dropped so that the speed enters merely as a parameter [19–21]. In the end, which collisionless terms to include in the drift-kinetic equation is effectively a choice between different particle trajectories. Another common approximation is to only retain pitch-angle scattering collisions, which implies that coupling in the energy dimension is eliminated and that momentum is generally not conserved.

In contrast SFINCS implements full linearized Fokker-Planck collisions, and allows for full particle trajectories including the true $\mathbf{E} \times \mathbf{B}$ drift. The code is adapted for an arbitrary number of species, allows for general non-axisymmetric nested flux surface geometry, and employs Boozer coordinates (Eq. (2.6)). As is customary in transport codes, SFINCS takes thermodynamic forces as input and calculates neoclassical fluxes as output. SFINCS is parallelized and a typical simulation has to be done on a supercomputer. Runs at low collisionality are particularly expensive due to the presence of an internal boundary layer between the trapped-passing regions of velocity space, which implies that a high reso-

lution is needed in the toroidal direction and a large number of Legendre polynomials are required to represent the distribution function.

## 3.3 Turbulent transport

The experimentally measured radial fluxes of particles and energy are usually greater than would be expected from collisional transport theory alone [9]. This enhanced "anomalous" transport is attributed to small-scale turbulent fluctuations called microinstabilities. These instabilities saturate at a low amplitude, compared to the average background quantities, due to nonlinear mechanisms. The fluctuating electric fields make the particles $\mathbf{E} \times \mathbf{B}$ drift radially in a random manner. The fluctuation amplitude is typically small, with $\delta n/n_0$ (ratio of fluctuating and mean parts of the density) being less than 1% in the core. Closer to the edge the amplitude of the fluctuations can be larger, but in this thesis the main focus is on core turbulence.

The number of different kinds of *modes* (or waves) that can exist in a plasma is large compared to vacuum where only electromagnetic waves can propagate [15]. In a Fourier description each mode is characterized by its wave vector $\mathbf{k}$ and frequency $\omega = \omega_r + i\gamma$, and the *dispersion equation* relating them. Any dynamical quantity $Q$ (e.g. density, pressure, velocity, electric potential,...) can be represented in the form $Q = Q_0 + \delta Q$, where $Q_0 = \langle Q \rangle_{ens}$ is the ensemble average of $Q$ and $\delta Q$ is a deviation from $Q_0$ (the fluctuation). In a linear description, where the perturbations remain small, $\delta Q \propto \exp(i\mathbf{k} \cdot \mathbf{r} - i\omega t)$. Then $\omega_r$ is the fluctuation frequency while $\gamma$ is either the damping rate, if $\gamma < 0$, or growth rate, if $\gamma > 0$. The latter case characterizes an unstable mode. For a linearly unstable mode, the amplitude of $\delta Q$ will grow in time, and therefore the nonlinear terms (previously neglected) will become more important and lead to interactions between several linear modes. This generally leads to a complex rearrangement of the plasma structure and the state becomes truly turbulent. The level of transport is determined by the saturation amplitude of the perturbed quantities and different saturation mechanisms will result in different diffusivities.

### 3.3.1 Microinstabilities

In a spatially inhomogeneous plasma, so-called *drift waves* appear. They are driven by the free energy source stored in the gradients, and play

a crucial role in the mechanism of anomalous transport. The free energy can become accessible for waves, which can then be destabilized. This can be provided through mechanisms such as unfavorable magnetic curvature and parallel compressibility. We can classify microinstabilities into various modes according to the variety of free energy sources, accessibility mechanisms and magnetic geometry. Two of the most important electrostatic drift wave types are the ion temperature gradient (ITG) mode and the trapped electron (TE) mode, and they will be further discussed in this thesis.

The microinstabilities have spatial scales which are typically significantly longer than the Debye length and are relatively slow, so that quasineutrality $\sum_\alpha e_\alpha \delta n_\alpha = 0$ (where $\delta n_\alpha$ is the perturbed density) is a good approximation. Quasineutrality can therefore be used to obtain an electrostatic dispersion relation from the density responses of the different species. Furthermore the microinstabilities have much lower frequencies than the gyro frequencies ($\Omega_e$, $\Omega_i$), and it is therefore appropriate to use gyro-averaged equations. Several types of microinstabilities also have lower frequency than the trapped electron bounce frequency, allowing for bounce averaged electron equations. As a consequence of this averaging operator the parallel dynamics is annihilated for trapped electrons.

When analyzing microinstabilities it is sometimes sufficient to focus on electrostatic perturbations and neglect magnetic field perturbations. In Appendix A of Ref. [15] an order-of-magnitude estimate is presented which shows that $\left(|\delta \mathbf{B}|/B\right)/\left(\delta n_e/n\right) \sim \beta$, and since $\beta$ is usually small we conclude that the electrostatic approximation is often valid. Still there are scenarios where $\beta$ can be relatively high and simulation codes often allow for the inclusion of magnetic field perturbations. In the present thesis the main focus is on electrostatic turbulence.

### Ion temperature gradient mode

As the name suggests the ITG mode is driven by the ion temperature gradient. High central ion temperature is a requirement for magnetic fusion and therefore large temperature gradients will be present. The ITG modes are of primary interest and believed to be the major contributor to anomalous ion thermal transport. The ITG modes primarily arise due to bad magnetic curvature, destabilized by $\nabla B$ and curvature drifts, or by resonant parallel ion dynamics. In the former case the mode is called the toroidal ITG mode since it is related to the geometry, while in the

latter case it is called the slab ITG and appears even if the magnetic curvature is neglected.

The toroidal ITG mode can be interpreted as follows. The bad magnetic curvature of a tokamak is on the outboard, low-field side of the torus. If a temperature perturbation emerges there, the fast magnetic drift of particles have different velocities in different temperature regions. This leads to a growing density perturbation, out of phase with the temperature perturbation. As a consequence of the density perturbation, a potential perturbation is generated leading to $\mathbf{E} \times \mathbf{B}$ drift flows. The phase between the perturbed flows and the temperature perturbation is such that hot plasma is transported to the high temperature parts of the perturbation. This results in a feedback mechanism leading to a growing perturbation amplitude, and thus an instability. On the inboard side of the torus, the direction of $\nabla T$ is opposite to that of $\nabla B$, and the feedback mechanism disappears. The dependence of the ITG drive (and thus the fluctuation amplitude) on poloidal angle is one of the reasons why it typically has the "ballooning" form of the mode structure.

A toroidal ITG mode typically has a frequency of $\omega \sim k_\theta \rho_i v_{Ti}/R$, where $k_\theta$ is the poloidal mode number and $v_{Ti}$ the thermal ion velocity. It propagates in the ion diamagnetic direction. When the mode frequency falls below the trapped ion bounce frequency, $\omega_{bi} = v_{Ti}\sqrt{\epsilon}/\left(qR\right)$, trapped ion effects become destabilizing and the mode gradually evolves into a trapped ion mode (TIM).

### Trapped electron mode

When the mode frequency is comparable to or lower than the trapped particle bounce frequency, trapping effects become important. Trapped particles spend most of their time in the bad curvature region on the low field side of a torus, thus the magnetic curvature drift is not averaged out as it is for passing particles. Local electric fields arise leading to $\mathbf{E} \times \mathbf{B}$ drifts and resulting in microinstabilities.

The trapped electron response is the dominant contribution to the non-adiabatic electron response [22]. Therefore the TE mode, primarily driven by the trapped electron toroidal precession resonance, is of interest. The TE modes appear in the same wave number range as the ITG modes, $k_\theta \rho_i \lesssim 1$, and with a similar frequency. TE modes can be the dominant instabilities in scenarios where $\eta_i \equiv d\ln T_i/d\ln n_i$ is small, so that ITG modes do not occur, and if the effective electron collisionality $\nu_{\text{eff}}$ is low enough. Frequent collisions would lead to de-trapping of the

trapped electrons within a bounce period and thus to removal of the trapped electron drive. The TE modes are typically driven by the density gradients $1/L_n$ and/or the electron temperature gradient $1/L_{Te}$. Unlike ITG modes, TE modes propagate in the electron diamagnetic direction.

TE modes can be divided into the dissipative (DTEM) and collisionless (CTEM) classes. In the former, energy is transferred from trapped electrons to waves via trapped electron collisions, and a strong electron temperature gradient and high collisionality are required. Still the collisionality has to be low enough for the trapped electrons to execute a bounce period before being de-trapped. On average the typical trapped electrons are de-trapped by collisions during one wave period but not during the shorter bounce motion period. In the latter class, energy is transferred to waves through wave-precession-drift resonance, and therefore this class is more likely to be destabilized in reactor relevant conditions, where the collisionality will be low. Collisions must be rare enough for trapped electrons to precession drift around the torus more than once before being de-trapped by collisions. The collisionless TE mode is investigated carefully in paper C and shown to be stabilized by increasing collisionality.

### 3.3.2 Theoretical description

#### Adiabatic response

Since electrons can adjust quickly to potential variations, due to their high velocity, a common approximation to make is the Boltzmann response for the electron density

$$\frac{\delta n_e}{n_0} = \frac{|e|\,\delta\phi}{T_e}, \tag{3.29}$$

where $\delta\phi$ is the fluctuating electrostatic potential (note that in the papers we often refer to this simply as $\phi$). This is called the adiabatic response because of the reference to the relative slow timescale of a drift wave compared to the electron transit motion, $\omega \ll k_\parallel v_{Te}$ where $v_{Te}$ is the thermal electron velocity and $k_\parallel$ the parallel wave number. Note that, unlike electron drift waves, ITG modes can be driven unstable even with an adiabatic electron response. A typical consequence of the adiabatic assumption is, as we will see later, that no cross-field transport results.

### Gyrokinetic description

The gyrokinetic framework is particularly suitable to describe turbulent fluctuations in plasmas, and the approach is based on the assumption that the equilibrium quantities are slowly varying, while the perturbations are smaller but more rapidly varying in space. The idea of gyrokinetics is that on the time scales and length scales of interest (here for the turbulent fluctuations), it is typically not necessary to follow the rapid gyro motion of particles, but rather look at the distribution of the guiding centers. The equations can therefore be averaged over the gyro-phase, thus reducing the description from a 6D phase-space to 5D. The equations can advantageously be derived using a different coordinate system, such as guiding center coordinates $(\mathbf{R}, \mathcal{E}, \mu, \zeta)$, and in different magnetic geometries. Here we are naturally most interested in the toroidal geometry. These equations can be derived using a recursive technique. The equations presented in the present section are based on [23, 24]. A thorough review of gyrokinetic theory is presented in Ref. [25].

As mentioned earlier, the fields can be decomposed into an ensemble average and a fluctuation

$$\begin{aligned} \mathbf{E} &= \mathbf{E}_0 + \delta\mathbf{E}, \qquad & \phi &= \phi_0 + \delta\phi, \\ \mathbf{B} &= \mathbf{B}_0 + \delta\mathbf{B}, \qquad & \mathbf{A} &= \mathbf{A}_0 + \delta\mathbf{A}, \end{aligned} \tag{3.30}$$

with $\mathbf{E} = -\nabla\phi - \partial\mathbf{A}/\partial t$ and $\mathbf{B} = \nabla \times \mathbf{A}$ (in the electrostatic approximation $\delta\mathbf{B} = \delta\mathbf{A} = 0$). Similarly the distribution function of species $\alpha$ is decomposed into

$$f_\alpha = F_\alpha + \delta f_\alpha, \tag{3.31}$$

where $F_\alpha$ is the ensemble-average of $f_\alpha$.

As in the drift-kinetic theory described in Sec. 3.2.1, the derivation of the gyrokinetic equation is based on an expansion of the Fokker-Planck equation in the smallness of $\rho_*$. However here often $\rho_* = \rho_s/a$ where $\rho_s = c_s/\Omega_i \sim \rho_i\sqrt{T_e/T_i}$ is the ion sound Larmor radius and $c_s = \sqrt{T_e/m_i}$ is the ion sound speed. The ordering of gyrokinetic theory is written as

$$\frac{\delta f_\alpha}{F_\alpha} \sim \frac{e_\alpha \delta\phi}{T_\alpha} \sim \frac{e_\alpha v_{T\alpha}\,|\delta\mathbf{A}|}{T_\alpha} \sim \frac{k_\parallel}{k_\perp} \sim \frac{\omega}{\Omega_\alpha} \sim \rho_*. \tag{3.32}$$

When the ensemble-averaged quantities change only due to fluxes driven by fluctuations of sizes described by Eq. (3.32), they must vary slowly as $\partial/\partial t \sim \rho_*^2$.

The Fokker-Planck equation (Eq. (3.2)) is written as

$$\left\{\frac{\partial}{\partial t}+\mathbf{v}\cdot\nabla+\frac{e_\alpha}{m_\alpha}\left[(\mathbf{E}_0+\delta\mathbf{E})+\mathbf{v}\times(\mathbf{B}_0+\delta\mathbf{B})\right]\cdot\frac{\partial}{\partial\mathbf{v}}\right\}(F_\alpha+\delta f_\alpha)= \\ =C_\alpha\left[F_\alpha+\delta f_\alpha\right]. \quad (3.33)$$

The general approach is to separate Eq. (3.33) into two components, the ensemble-average (equilibrium) part, $\mathcal{A}$, and the fluctuating (perturbed) part, $\mathcal{F}$,

$$\mathcal{A}=\left.\frac{d}{dt}\right|_{ens}F_\alpha-\langle C_\alpha\rangle_{ens}-\mathcal{D}_\alpha, \quad (3.34)$$

$$\mathcal{F}=\left.\frac{d}{dt}\right|_{ens}\delta f_\alpha+\frac{e_\alpha}{m_\alpha}(\delta\mathbf{E}+\mathbf{v}\times\delta\mathbf{B})\cdot\frac{\partial}{\partial\mathbf{v}}(F_\alpha+\delta f_\alpha)-C_\alpha+\langle C_\alpha\rangle_{ens}+\mathcal{D}_\alpha, \quad (3.35)$$

where

$$\left.\frac{d}{dt}\right|_{ens}\equiv\frac{\partial}{\partial t}+\mathbf{v}\cdot\nabla+\frac{e_\alpha}{m_\alpha}(\mathbf{E}_0+\mathbf{v}\times\mathbf{B}_0)\cdot\frac{\partial}{\partial\mathbf{v}},$$

$$\mathcal{D}_\alpha\equiv-\frac{e_\alpha}{m_\alpha}\left\langle(\delta\mathbf{E}+\mathbf{v}\times\delta\mathbf{B})\cdot\frac{\partial\delta f_\alpha}{\partial\mathbf{v}}\right\rangle_{ens}.$$

Now ensemble averages as well as fluctuations are expanded in powers of $\rho_*$

$$\begin{aligned}
&F_\alpha=F_{\alpha0}+F_{\alpha1}+F_{\alpha2}+\ldots,\\
&\mathbf{E}_0=\mathbf{E}_{00}+\mathbf{E}_{01}+\mathbf{E}_{02}+\ldots,\\
&\mathbf{B}_0=\mathbf{B}_{00},\\
&\delta f_\alpha=\delta f_{\alpha1}+\delta f_{\alpha2}+\ldots,\\
&\delta\mathbf{E}=\delta\mathbf{E}_1+\delta\mathbf{E}_2+\ldots,\\
&\delta\mathbf{B}=\delta\mathbf{B}_1+\delta\mathbf{B}_2+\ldots.
\end{aligned} \quad (3.36)$$

Note that we can put $\mathbf{B}_{01}=\mathbf{B}_{02}=\ldots=0$ because $\mathbf{B}$ is used as the basis for defining the expansion parameter $\rho_*$ [24], and also that $\mathbf{E}_{00}=-\nabla\phi_{00}$, $\mathbf{E}_{01}=-\nabla\phi_{01}$ because of the ordering $\partial\mathbf{A}/\partial t\sim\rho_*^2$. It is now possible to split Eq. (3.33) into different orders of $\rho_*$, and then use the gyro-phase average $\langle G(\mathbf{R},\zeta)\rangle_{\mathbf{R}}$.

Taking the gyro-phase average of the $0^{\text{th}}$ order ensemble-averaged equation, $\mathcal{A}_0=0$, gives the lowest order equilibrium distribution $F_{\alpha0}$ which is a Maxwellian (defined by Eq. (3.17)) in a rotating reference frame where the density can vary over a flux surface due to the centrifugal force. $\mathbf{V}_{\alpha0}$ in Eq. (3.17) is the purely toroidal mean flow velocity of the species. From now on we assume that on average the plasma is not

rotating toroidally and put $\mathbf{V}_{\alpha 0} = 0$. Continuing with gyro-averages of higher orders of the ensemble-averaged equation, $\mathcal{A} = 0$, results in different orders of the drift-kinetic equation.

From the gyro-average of the first order perturbed equation, $\mathcal{F}_1$, an expression for the first order fluctuating distribution, $\delta f_{\alpha 1}$, is obtained in terms of the distribution of the guiding centers $H_\alpha(\mathbf{R})$ as

$$\delta f_{\alpha 1}(\mathbf{r}) = -\frac{e_\alpha \delta\phi(\mathbf{r})}{T_\alpha} F_{\alpha 0} + H_\alpha(\mathbf{R}). \tag{3.37}$$

Here we can identify the first term on the right as the adiabatic response of the perturbed distribution, whereas the second term is consequently referred to as the non-adiabatic part. $H_\alpha(\mathbf{R})$ is determined by solving the nonlinear gyrokinetic equation.

It is now useful to introduce the function $h_\alpha(\mathbf{R}) = H_\alpha(\mathbf{R}) - e_\alpha F_{\alpha 0}\delta U(\mathbf{R})/T_\alpha$ with the gyro-averaged quantity

$$\delta U(\mathbf{R}) \equiv \langle \delta\phi(\mathbf{r}) - \mathbf{v}\cdot\delta\mathbf{A}(\mathbf{r})\rangle_{\mathbf{R}}. \tag{3.38}$$

The gyrokinetic equation is obtained from the next order perturbed equation and can, in an axisymmetric toroidal configuration with negligible toroidal rotation, be written as [23]

$$\frac{\partial h_\alpha}{\partial t} + \left(v_\parallel \mathbf{b} + \mathbf{v}_d\right)\cdot\nabla H_\alpha + \delta\mathbf{v}_d\cdot\nabla h_\alpha - C_\alpha[H_\alpha] = -\delta\mathbf{v}_d\cdot\nabla F_{\alpha 0}, \tag{3.39}$$

where $\mathbf{v}_d$ is the drift velocity given in Eq. (2.2) with the $\mathbf{E}\times\mathbf{B}$ drift velocity subtracted [23], and we have introduced the perturbed drift velocity $\delta\mathbf{v}_d = \mathbf{b}\times\nabla\delta U/B$.

To make the equations self-consistent and couple the response of different species to each other, we use the Poisson equation and Ampère's law. We introduce the scalar electromagnetic fields $\delta A_\parallel \equiv \mathbf{b}\cdot\delta\mathbf{A}$ and $\delta B_\parallel \equiv \mathbf{b}\cdot\nabla\times\delta\mathbf{A}$ and write:
Poisson equation

$$\nabla_\perp^2 \delta\phi(\mathbf{r}) = -\frac{1}{\epsilon_0}\sum_\alpha e_\alpha \int d^3v\, \delta f_\alpha(\mathbf{r},\mathbf{v}), \tag{3.40}$$

Ampère's law

$$\begin{aligned} \nabla_\perp^2 \delta A_\parallel(\mathbf{r}) &= -\mu_0 \textstyle\sum_\alpha e_\alpha \int d^3v\, v_\parallel \delta f_\alpha(\mathbf{r},\mathbf{v}) \\ \nabla_\perp \delta B_\parallel(\mathbf{r})\times\mathbf{b} &= \mu_0 \textstyle\sum_\alpha e_\alpha \int d^3v\, \mathbf{v}_\perp \delta f_\alpha(\mathbf{r},\mathbf{v}), \end{aligned} \tag{3.41}$$

where $\mu_0$ is the permeability of free space. We approximate the perturbed distribution as $\delta f_\alpha \approx \delta f_{\alpha 1}$ from the solution to the gyrokinetic equation (Eqs. (3.37) and (3.39)).

A common approach to solve space-time differential equations is to transform the problem into Fourier space. Then the equations can transform into a purely algebraic equation. However, searching for a solution to Eq. (3.39) this method leads to difficulties due to products of spatially-dependent quantities appearing in the equation, and Fourier transformation does not lead to an algebraic equation. Instead it is assumed that the fluctuating fields can be written as a superposition of components in the following form,

$$\delta Q\left(t, \mathbf{r}\right) = \sum_{\mathbf{k}_\perp} \delta \tilde{Q}_{\mathbf{k}_\perp}\left(t, \mathbf{r}\right) \exp\left(i\mathbf{k}_\perp \cdot \mathbf{r}\right), \tag{3.42}$$

where $\exp\left(i\mathbf{k}_\perp \cdot \mathbf{r}\right)$ represents rapid variations in the direction perpendicular to the magnetic field, recalling the ordering $k_\parallel / k_\perp \sim \rho_*$. The perpendicular wave vector $\mathbf{k}_\perp$ and $\delta \tilde{Q}_{\mathbf{k}_\perp}(t, \mathbf{r})$, as well as the ensemble-average $Q_0$, are assumed to be slowly spatially varying, i.e. $\delta \tilde{Q}_{\mathbf{k}_\perp}(t, \mathbf{r}) \approx \delta \tilde{Q}_{\mathbf{k}_\perp}(t, \mathbf{R})$. Using this (and recalling that $\mathbf{r} = \mathbf{R} + \boldsymbol{\rho}$) the gyro-average of one spectral component is found to be

$$\left\langle \delta \tilde{Q}_{\mathbf{k}_\perp}(t, \mathbf{R}) \exp\left(i\mathbf{k}_\perp \cdot \mathbf{r}\right) \right\rangle_{\mathbf{R}} = \delta \tilde{Q}_{\mathbf{k}_\perp}(t, \mathbf{R}) \exp\left(i\mathbf{k}_\perp \cdot \mathbf{R}\right) \left\langle \exp\left(i\mathbf{k}_\perp \cdot \boldsymbol{\rho}\right) \right\rangle_{\mathbf{R}}. \tag{3.43}$$

Gyro-averages can be evaluated in terms of the Bessel functions $J_m$ ($m \in \mathbb{Z}$) which can be defined through

$$J_m\left(\varrho\right) = \frac{1}{2\pi} \oint d\tau \exp\left(-im\tau + i\varrho \sin\tau\right), \tag{3.44}$$

and it is possible to show that e.g.

$$\left\langle \exp\left(i\mathbf{k}_\perp \cdot \boldsymbol{\rho}\right) \right\rangle_{\mathbf{R}} = J_0\left(k_\perp \rho_\alpha\right). \tag{3.45}$$

Utilizing the gyro-averages of other terms of the form $\left\langle \cdots \exp\left(i\mathbf{k}_\perp \cdot \boldsymbol{\rho}\right) \right\rangle_{\mathbf{R}}$ it is possible to rewrite $\delta U\left(\mathbf{R}\right)$ (defined in Eq. (3.38)) as

$$\delta U\left(\mathbf{R}\right) = J_0\left(k_\perp \rho_\alpha\right) \left[\delta\phi\left(\mathbf{R}\right) - v_\parallel \delta A_\parallel\left(\mathbf{R}\right)\right] + \frac{v_\perp^2}{2\Omega_\alpha} \left[J_0\left(k_\perp \rho_\alpha\right) + J_2\left(k_\perp \rho_\alpha\right)\right] \delta B_\parallel\left(\mathbf{R}\right). \tag{3.46}$$

The Bessel functions represent the finite Larmor radius (FLR) effects. A possible approximation in the electrostatic case, when only $J_0$ appears, is to neglect them by putting $J_0\left(k_\perp \rho_\alpha\right) = 1$.

In the local approximation, each Fourier harmonic $\delta\tilde{Q}_{\mathbf{k},\omega} \exp\left(i\mathbf{k}\cdot\mathbf{r} - i\omega t\right)$ of the perturbations $\delta Q\left(t,\mathbf{r}\right) = \sum_{\mathbf{k},\omega} \delta\tilde{Q}_{\mathbf{k},\omega} \exp\left(i\mathbf{k}\cdot\mathbf{r} - i\omega t\right)$ is assumed to be independent of the other harmonics, while in reality physical inhomogeneities may couple them [22]. Nonlocal treatments take this coupling into account, hence the nonlocal eigenmode is a superposition of many coupled Fourier harmonics.

In linear gyrokinetic theory the term $\delta\mathbf{v}_d \cdot \nabla h_\alpha$, containing products of fluctuating quantities, is neglected in Eq. (3.39). This reduces the complexity substantially, but still the equations are not possible to solve analytically even in the simplest toroidal geometry. Solving them numerically is often performed only by searching for the single most unstable eigenmode.

As a last remark of this section we mention that further on in this thesis perturbed quantities can also be denoted by $\hat{}$ (e.g. $\delta n_\alpha = \hat{n}_\alpha$), and the $0^{\text{th}}$ order equilibrium distribution is simply denoted by $f_{\alpha 0}$ (instead of $F_{\alpha 0}$). In ballooning space the non-adiabatic part of the perturbed distribution is denoted by $g$ and the perturbed potential by $\phi$.

### 3.3.3 Ballooning formalism

Turbulent fluctuations in magnetic fusion plasmas are typically highly elongated along magnetic field lines, but have a short perpendicular scale [26, 27]. The parallel and perpendicular wave numbers satisfy $k_\parallel \sim 1/\left(qR\right) \ll k_\perp$ with $k_\perp \rho_i \sim 1$. Perturbations are usually written as a superposition of components (after separating the time dependence $e^{-i\omega t}$) according to $\delta Q\left(r,\theta,\varphi\right) = \sum_{n,m} \delta\tilde{Q}_{n,m}\left(r\right) e^{i(m\theta - n\varphi)}$ [28], but in toroidal geometry the poloidal components are coupled (compare to Eq. (3.42)) and the perturbation is written

$$\delta Q\left(r,\theta,\varphi\right) = \sum_{n,m} \delta\tilde{Q}_{n,m}\left(r,\theta\right) e^{i(m\theta - n\varphi)}. \tag{3.47}$$

Here we use $n, m \in \mathbb{Z}$ for the toroidal and poloidal mode numbers respectively, related to $k_\varphi$, $k_\theta$ by $k_\varphi = -n/R$ and $k_\theta = m/r$. Note that with this representation $\delta\tilde{Q}_{n,m}\left(r,\theta\right)$ has to be $2\pi$-periodic in $\theta$. The tokamak has unfavorable magnetic curvature on the outboard side, implying that many instabilities are more easily excited at that location. This results in a ballooning structure of the fluctuations, where the perturbations

are largest in amplitude close to $\theta = 0$. Because of this ballooning-like structure, it is not efficient to represent perturbations according to Eq. (3.47). We are interested in a set of mode numbers such that $m = nq$, but then the representation of $\delta Q$ in Eq. (3.47) is only useful on a flux surface where $q$ is a rational number since the perturbation should be $2\pi$-periodic in $\theta$ and $\varphi$. For non-zero magnetic shear $q$ is irrational at an infinitesimal distance away from a rational surface.

Because of the elongated linear mode structure $nq$ is large, which implies that the rational surfaces are close to each other. Hence the microinstabilities radially extend over several rational surfaces rather than being localized around one. It is thus more convenient to write the perturbation in the ballooning representation [26, 29], appropriate for describing mode structures characterized by long parallel wavelength and short perpendicular wavelength when the magnetic shear is finite. The $n^{\text{th}}$ toroidal harmonic of the perturbation can be expressed as $\delta Q_n(r,\theta,\varphi) = \delta\tilde{Q}_{n,m}(r,\theta)\, e^{-in[\varphi - q(r)\theta]}$. We rewrite this harmonic in terms of an extended poloidal angle $\vartheta = \theta + 2\pi j \in \mathbb{R}$ $(j \in \mathbb{Z})$ as

$$\delta Q_n(r,\theta,\varphi) = \sum_{\theta_0} \sum_{j=-\infty}^{\infty} \delta\tilde{Q}_{B,n}(\vartheta,\theta_0)\, e^{-in[\varphi - q(r)(\vartheta+\theta_0)]}, \tag{3.48}$$

where the ballooning angle $\theta_0$ has been introduced. $\vartheta$ is basically a coordinate along the field line, while $\theta_0$ is the real poloidal angle where the wave fronts are perpendicular to the flux surface. $\delta\tilde{Q}_{B,n}(\vartheta,\theta_0)$ does not have a periodicity condition, only the requirement that $\delta\tilde{Q}_{B,n}(\vartheta,\theta_0)$ $\to 0$ as $|\vartheta| \to \infty$. To calculate the most unstable mode it is usually enough to consider the $\theta_0 = 0$ term, so for practical purposes we can make the approximation

$$\delta Q_n(r,\theta,\varphi) \approx \sum_{j=-\infty}^{\infty} \delta\tilde{Q}_{B,n}(\vartheta)\, e^{-in[\varphi - q(r)\vartheta]}, \tag{3.49}$$

where $\delta\tilde{Q}_{B,n}(\vartheta) \equiv \delta\tilde{Q}_{B,n}(\vartheta,0)$.

In the ballooning representation the eigenmodes are radially periodic, which means that it is only a realistic representation if the plasma parameters are constant over the considered radial domain. Making this approximation can be justified in the $\rho_* \to 0$ limit, i.e. when the plasma size is much larger than the radial domain. This is called flattening of the profiles, and is often used in simulations to reduce the computational task.

### 3.3.4 Gyrokinetic equation in ballooning space

The linearized gyrokinetic equation for the non-adiabatic part of the perturbed distribution $g_\alpha$ is in ballooning space given by (i.e. $g = g_{B,n}(\vartheta)$) [30]

$$\frac{v_\parallel}{qR}\frac{\partial g_\alpha}{\partial \vartheta}\bigg|_{\mathcal{E},\mu} - i(\omega - \omega_{D\alpha} - \omega_E)g_\alpha - C[g_\alpha] = -i\frac{e_\alpha f_{\alpha 0}}{T_\alpha}\left(\omega - \omega_{*\alpha}^T\right)\phi J_0(z_\alpha), \tag{3.50}$$

for a low-$\beta$, circular cross section, axisymmetric, large aspect ratio equilibrium and in the presence of a poloidally varying equilibrium potential $\phi_E$, where only pure electrostatic perturbations are considered ($\phi(\vartheta)$ is the perturbed potential in ballooning space) and we neglect plasma rotation. Note that the time derivative is expressed in terms of wave frequency, i.e. $\partial/\partial t \to -i\omega$. Here $f_{\alpha 0} = n_{\alpha 0}(m_\alpha/2\pi T_\alpha)^{3/2}\exp(-\mathcal{E}/T_\alpha)$ is an equilibrium Maxwellian distribution function, $n_\alpha(\mathbf{r}) = n_{\alpha 0}\exp[e_\alpha\phi_E(\mathbf{r})/T_\alpha]$ is the poloidally varying density and $n_{\alpha 0}$ is a flux function. The diamagnetic frequency is defined as $\omega_{*\alpha} = -k_\theta T_\alpha/e_\alpha B L_{n\alpha}$ and $\omega_{*\alpha}^T = \omega_{*\alpha}\left[1 + \left(x^2 - 3/2\right)L_{n\alpha}/L_{T\alpha}\right]$, where $x = v/v_{T\alpha}$ represents velocity normalized to the thermal speed $v_{T\alpha} = (2T_\alpha/m_\alpha)^{1/2}$. The magnetic drift frequency is $\omega_{D\alpha} = -2k_\theta T_\alpha(x_\perp^2/2 + x_\parallel^2)\mathcal{D}(\vartheta)/(m_\alpha\Omega_\alpha R)$, with $\mathcal{D}(\vartheta) = \cos\vartheta + s\vartheta\sin\vartheta$. The argument of the Bessel function is $z_\alpha = k_\perp v_\perp/\Omega_\alpha$, with $k_\perp = \left(1 + s^2\vartheta^2\right)^{1/2}k_\theta$, and it is responsible for the FLR effects. The $\mathbf{E}\times\mathbf{B}$ drift frequency of the particles in the equilibrium electrostatic field is $\omega_E = -\dfrac{k_\theta}{B}\dfrac{s\vartheta}{r}\dfrac{\partial\phi_E}{\partial\vartheta}$, and was derived in Appendix A of paper A. Note that usually this term is left out of the equation, because it only exists if there is a local poloidal (or radial) variation in the equilibrium potential which can often be neglected. However under certain conditions, and in particular when describing high-$Z$ impurities, its magnitude can be comparable to the other terms and thus it has to be included. The first term on the left of Eq. (3.50), is referred to as the parallel compressibility (or parallel dynamics). Sometimes this term does not affect the linear mode frequency significantly, and it is therefore common in simulation packages to allow for the possibility of neglecting it. This can e.g. be used when studying the toroidal ITG mode mentioned in Sec. 3.3.1, but it can also be advantageously used to study the impact of the term itself. Although ignoring parallel compressibility can lead to reasonable estimates for linear growth rates, this simplification does not give the correct nonlinear evolution of modes [22], and should thus only be considered for linear simulations. Much of the work in this

thesis is based on Eq. (3.50), and we will return to it further on.

### 3.3.5 Turbulent fluxes

The overriding goal of transport theory in magnetic fusion plasmas is to determine the cross-field fluxes of e.g. particles and energy. These fluxes can be theoretically divided into collisional and anomalous components, e.g. $\Gamma = \Gamma_{\mathrm{CO}} + \Gamma_{\mathrm{AN}}$, where the anomalous component often dominates over the collisional. The anomalous component represents the ensemble-average of the flux due to turbulent fluctuations [15].

Focusing on electrostatic turbulence, a potential perturbation $\delta\phi$ gives rise to a perturbed drift velocity $\delta\mathbf{v}_d = \mathbf{b} \times \nabla \delta U/B$ with $\delta U = \delta\phi$ from Eq. (3.38). This produces a particle flow, which can be averaged over a flux surface to obtain the cross-field particle flux through the surface $\Gamma_{\alpha\perp}$ as [24, 28]

$$\Gamma_{\alpha\perp} = \langle \mathrm{Re}\left[\delta n_\alpha \delta \mathbf{v}_d^* \cdot \nabla r\right] \rangle \,, \tag{3.51}$$

where $\mathrm{Re}\left[\cdots\right]$ denotes the real part and $^*$ the complex conjugate. The perturbed density is obtained by taking the $0^{\mathrm{th}}$ moment of the perturbed distribution function, consequently it can be seen from Eq. (3.50) (recall that $\phi$ in Eq. (3.50) corresponds to $\delta\phi$ here) that $\delta n_\alpha \propto \delta\phi$. This can also be verified from Eq. (3.39) in the nonlinear case. This proportionality is also true for the temperature perturbation since it is a higher order moment of the same perturbed distribution. We now note that we can use $\delta\mathbf{v}_d^* \cdot \nabla r = \mathbf{b} \times \nabla \delta\phi^*/B \cdot \nabla r = ik_\theta \delta\phi^*/B$ to rewrite Eq. (3.51) and obtain the particle flux as

$$\Gamma_{\alpha\perp} = -\left\langle \frac{k_\theta}{B} \mathrm{Im}\left[\delta n_\alpha \delta\phi^*\right] \right\rangle , \tag{3.52}$$

where $\mathrm{Im}\left[\cdots\right]$ denotes the imaginary part. Similarly the energy flux is found to be

$$Q_{\alpha\perp} = -\left\langle \frac{k_\theta}{B} n_\alpha \mathrm{Im}\left[\delta T_\alpha \delta\phi^*\right] \right\rangle . \tag{3.53}$$

From Eq. (3.51) we make the important observation, that if the "transporter" $\delta\mathbf{v}_d$ and the "transportee" $\delta n_\alpha$ are 90° out of phase there is no net transport of particles. Equivalently Eqs. (3.52) and (3.53) reveal that turbulent particle (energy) fluxes only occur when the perturbed density (temperature) and the perturbed potential are out of phase. This leads to the immediate conclusion that the adiabatic response, described by Eq. (3.29), does not contribute to the cross-field particle fluxes.

As mentioned earlier, linear gyrokinetic theory is implemented by neglecting all terms in the gyrokinetic equation containing products of fluctuating quantities. The anomalous fluxes obtained in this theory are referred to as the *quasilinear* fluxes [15]. In linear theory only the most unstable mode is usually analyzed (although it is possible to search for sub-dominant modes). If an instability exists, the linear growth rate $\gamma > 0$ and the perturbed quantities $\delta Q \propto \exp\left(i\mathbf{k}\cdot\mathbf{r} - i\omega_r t + \gamma t\right)$ grow exponentially in time indefinitely. We realize that such a behavior is unphysical. As the fluctuating amplitudes increase, saturation from nonlinear mode-coupling becomes more and more important, and the linear approximation breaks down. A consequence of this is that it is not possible to calculate the absolute anomalous fluxes from a linear approach, to do that one has to resort to nonlinear transport theory. To estimate the fluxes in quasilinear transport theory a common approach is to estimate the magnitude of the perturbed potential based on a so-called *mixing length* approximation. This procedure is a crude way of associating an instability with a random walk picture [15].

As a final remark of this section, we note that in a local flux-tube limit (described in Sec. 3.3.6) one can prove, by summing the averaged particle fluxes over species and using Maxwell's equations, that the anomalous fluxes possess the ambipolarity property given by Eq. (3.28) [23, 24]. Ambipolarity implies that on average the electric current is zero in the cross-field direction.

### 3.3.6 Gyrokinetic simulations

Today several different packages exist to simulate radial anomalous transport from microturbulence in tokamaks using the gyrokinetic approach; both particle-in-cell codes and continuum codes are available. In the local approximation they commonly work by specifying plasma parameters such as the geometry and local gradients, as well as the temporal and spatial domain, resolution of the simulation, number of eigenmodes and mode numbers, etcetera. The computed outputs are the perturbed quantities, the mode frequencies and turbulent fluxes. The simulation domain is typically a flux tube following the magnetic field lines, with a radial and binormal extent. The domain size in all three spatial dimensions has to be significantly larger than the correlation length of the turbulence. For this type of domain it is convenient to use a field aligned coordinate system. The plasma parameters and gradients can be approximated as constants over the perpendicular simulation domain in

the limit $\rho_* \to 0$. Local flux-tube simulations normally use periodic radial boundary conditions, while global simulations allow for non-periodic boundary conditions and can be useful for analyzing e.g. non-local effects.

Linear gyrokinetic simulations typically only search for one toroidal eigenmode, which grows exponentially and never saturates due to the absence of nonlinear mode-coupling. This implies that it is not possible to calculate the magnitude of the perturbed quantities, and thus neither the absolute fluxes, in contrast to nonlinear simulations. However it is still possible to determine if the analyzed mode contributes to inward or outward radial transport linearly, i.e. in the absence of mode-coupling. Linear simulations usually use an initial value technique to find the most unstable mode, but it can also be possible to search for sub-dominant modes using eigenvalue solvers.

Nonlinear simulations are run until the system reaches a state of fully developed turbulence, when the fluctuating quantities have reached an amplitude where nonlinear mode coupling becomes important. This state is statistically independent of the initial conditions. After reaching the turbulent state, the simulation has to continue running long enough for the statistical properties of the output quantities to be correctly determined.

Gyrokinetic simulation of turbulent transport is a heavy numerical task. Nonlinear simulations typically require vast computer resources to produce good statistics. Today's rapid development of supercomputers has enabled a more extensive utilization of gyrokinetic simulations, but still it is a tedious task to produce large numbers of nonlinear results. Linear simulations are significantly less expensive, and can in several situations be used for qualitative predictions. To calculate turbulent fluxes it can be useful to resort to fluid simulations which, despite not being as accurate, normally are much faster than nonlinear gyrokinetic simulations.

In the present thesis results are obtained from simulations with GYRO [31, 32]. GYRO, developed at General Atomics, USA, is a nonlinear tokamak microturbulence package using a fixed Eulerian grid to solve the 5D gyrokinetic-Maxwell equations. It is able to treat a local flux-tube domain or a global radial domain in a full or partial torus with a general shaped plasma cross section.

## 3.4 Impurity transport

In the core of a fusion plasma the fusion reactivity should be high. Since impurities lead to plasma dilution and radiative energy losses, impurity accumulation in the core must be avoided. As mentioned earlier high-$Z$ impurities are particularly detrimental.

It is widely accepted that the cross-field transport in tokamaks is usually dominated by turbulent transport and that the collisional transport is significantly smaller (e.g. see Ref. [33] and Paper E for comparisons of turbulent and collisional transport levels). However, in a stellarator the two transport channels could be comparable and in low-collisionality high-temperature plasmas the collisional transport can even dominate [10, 11]. In this thesis we analyze collisional impurity transport in stellarator plasmas and turbulent impurity transport in tokamak plasmas.

As discussed in Sec. 3.2.3, the radial electric field $E_r$ enters as a thermodynamic force in a stellarator. $E_r$ is important for the impurity transport, particularly since its impact is proportional to the impurity charge. In the usual situation, $E_r$ points in the direction which leads to impurity accumulation. This is a problem for stellarators, and can eventually be a showstopper when it comes to building reactor relevant devices. The search for scenarios where the impurity accumulation can be mitigated is thus an important endeavor of the stellarator community.

In recent years it has been observed experimentally that plasma heating by radiofrequency (RF) waves close to the center can result in a reduction of the impurity content in the core of a tokamak plasma (see Fig. 3.2) [34]. This is an effect which lacks a complete theoretical understanding, but could possibly be connected to a poloidal redistribution of the impurity species over a flux surface. This redistribution has been observed experimentally in tokamaks (see Fig. 3.2) [35]. Reference [36] includes an explanation of how an impurity species can become poloidally asymmetrically distributed under ICRH of a minority species, and [37] presents a theoretical model for the link between the asymmetry strength and the ICRH.

This thesis partially addresses the topic of turbulent cross-field transport of high-$Z$ impurities present in trace quantities $Zn_z/n_e \ll 1$ in a tokamak, including the situation when a poloidally varying equilibrium potential $\phi_E$ is present. The trace limit is experimentally relevant, and implies that the turbulent modes driving the transport are unaffected by the presence of the impurities. When larger quantities of impurities are present however they can affect the structure of the

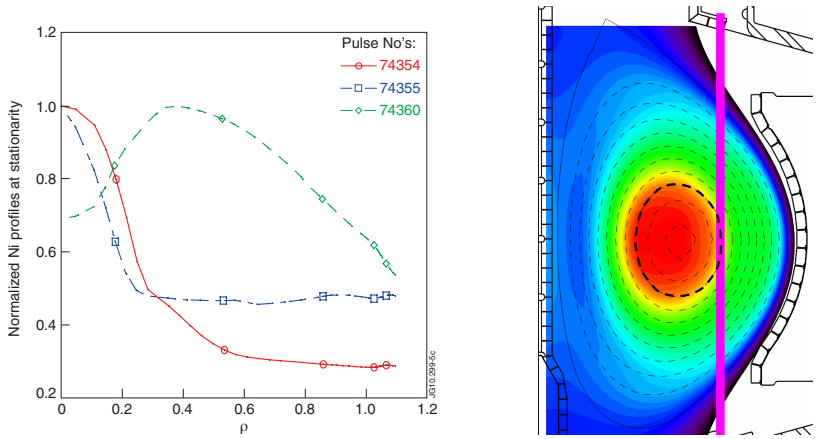


**Figure 3.2:** The left figure shows the normalized nickel density profiles (here $\rho$ is the radial coordinate) for three discharges in the JET tokamak with no heating power (74354), 1 MW (74355) and 3 MW (74360) of ICRH, respectively (figure from [34]). The right figure illustrates how applying ICRH with the resonance location at the low-field-side (highlighted with pink line), can lead to a poloidally asymmetrically distributed impurity species in the Alcator C-Mod tokamak (courtesy of M. L. Reinke).

turbulence. A model for $\phi_E$ is introduced as Eq. (11) of Paper A. This model implies that the impact of the poloidal variation is mainly on high-$Z$ impurities due to their high charge, while the main species remain almost unaffected. As a consequence we can obtain the eigenvalues $\omega$ and the perturbed potential $\phi$ of the most unstable mode from linear gyrokinetic simulations with GYRO, neglecting the varying equilibrium potential. The solution is substituted into Eq. (3.50) to give $g_z$. To analyze the turbulent radial impurity transport we calculate the zero-flux impurity density gradient (the peaking factor) obtained by requiring that the flux surface averaged linear impurity flux $\Gamma_z$ should vanish, $0 = \langle \Gamma_z \rangle \equiv -\left\langle \mathrm{Im}\left[\frac{k_\theta}{B}\hat{n}_z\phi^*\right]\right\rangle = -\left\langle \mathrm{Im}\left[\frac{k_\theta}{B}\int d^3v J_0\left(z_z\right) g_z\phi^*\right]\right\rangle$, where $\hat{n}_z$ here is the perturbed impurity density. In other words, the peaking factor $a/L^0_{nz}$ represents the (normalized) impurity density gradient in a steady state far from impurity sources, where a negative value implies that the impurity density increases in the radial direction (see Fig. 3.3). Consequently it is interesting to look for scenarios where the peaking factor is negative close to the plasma core.

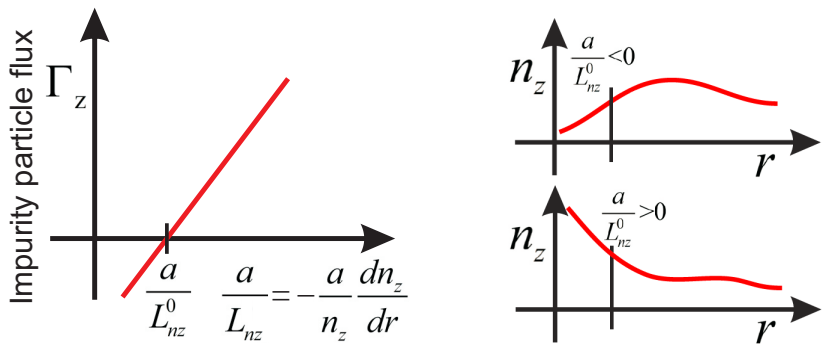


**Figure 3.3:** The left figure illustrates the definition of the impurity peaking factor $a/L_{nz}^0$ as the value of $a/L_{nz}$ when $\langle \Gamma_z \rangle = 0$. The right figure shows how the local impurity density varies when $a/L_{nz}^0 < 0$ and $a/L_{nz}^0 > 0$ respectively. If $a/L_{nz}^0 \geq 0$ everywhere inside the tokamak plasma, the impurity density profile is peaked. Otherwise it is hollow.

# Chapter 4

# Summary and conclusions

The present thesis treats aspects of radial transport of impurities in fusion devices. In particular we study turbulent impurity transport in axisymmetric devices (papers A–E) and collisional impurity transport in non-axisymmetric devices (papers F–G). The main part of the turbulent transport studies is devoted to quasilinear modelling of electrostatic turbulence. Furthermore, the role of a flux-surface varying non-fluctuating electrostatic potential in radial transport is explored. The main results of the papers are summarized below, and we close with an outlook on potential applications and directions for further studies.

In paper A electrostatic impurity core transport in the presence of a poloidally varying equilibrium potential $\phi_E$ is studied. This potential introduces a non-negligible modification to the particle orbits in the GK equation for high-$Z$ impurities, in the form of an $\mathbf{E} \times \mathbf{B}$-drift. A simple sinusoidal model for $\phi_E$ is suggested as $Ze\phi_E/T_z = -\kappa \cos(\theta - \delta)$, based on the effect of minority ion redistribution over a flux surface when applying ICRH on the low field side. Here $\kappa$ is the asymmetry strength, depending on e.g. heating power and resonance location, while $\delta$ is the angular position of the impurity maximum ($\delta = \pi$ in the case of low field side ICRH). We assume that $e\phi_E/T_\alpha \ll 1$ implying that the main species are almost unaffected by the varying potential, while $Ze\phi_E/T_z \sim \mathcal{O}(1)$ so that the impurities are affected due to their high charge. Moreover, we assume trace impurities ($Zn_z/n_e \ll 1$) which justifies that the eigenvalues and perturbed potential of the most unstable mode are obtained by linear gyrokinetic flux-tube simulations with the GYRO code in the poloidally symmetric case, assuming large-aspect ratio and circular cross section. Collisions are modeled by a Lorentz operator.

The solution from GYRO is substituted into the linearized GK equation for impurities, which is then solved using a variational approach.

The results suggest that the poloidal asymmetry strength and magnetic shear are the two most important parameters that affect the impurity peaking. A strong enough asymmetry can even lead to a negative impurity density gradient in steady state, which would imply that impurity accumulation in the core of a tokamak could be avoided. Our results indicate that these conclusions are general for any high-$Z$ impurity species present in trace quantities. It should be noted that in this particular work the parallel dynamics of main ions and impurities are neglected to simplify the analytical treatment. Furthermore FLR effects for the impurities are omitted by setting $J_0(z_z) = 1$.

Paper B extends the work of Paper A by analyzing the same baseline case but keeping the ion/impurity parallel dynamics, the FLR effects and using the more sophisticated linearized impurity-impurity collision operator $C_{zz}^{(l)}$ (the ordering $n_z Z^2/n_e \sim \mathcal{O}(1)$ implies that impurity self-collisions dominate over collisions with unlike species). A perturbative solution to Eq. (3.50) in the small parameter $Z^{-1/2}$ is constructed, keeping terms up to $\mathcal{O}\left(Z^{-1}\right)$. The subsequent semi-analytical expression (Eq. (8) in paper B) for the impurity peaking factor interestingly shows that up to order $Z^{-1}$ the peaking is independent of both FLR effects and collisionality, except for indirect effects from the main species in the mode characteristics. This expression essentially shows that the impurity peaking is determined by three separate contributions: one coming from the magnetic drifts, another from the $\mathbf{E} \times \mathbf{B}$ drift in the poloidally varying equilibrium potential, and a third arising due to the parallel impurity dynamics. Because of its explicit dependence on the mode frequency, this last contribution typically leads to an increased impurity peaking for ITG turbulence while the opposite could be expected for TE turbulence, in accordance with earlier fluid results.

In paper C the analysis is focused on collisionless TE modes driven by the density gradients or the electron temperature gradient, and the paper includes a thorough investigation of how these instabilities impact the radial impurity transport. The main part of the work is devoted to quasilinear studies and the same approximate solution for the impurity peaking factor is used as in paper B. To estimate the validity of the linear results, nonlinear GYRO simulations are performed and found to conform rather well with the linear simulations. Although the poloidally varying equilibrium potential (and the arising $\mathbf{E} \times \mathbf{B}$ drift) is still in-

cluded in the analysis, much of the attention of the paper is focused on the contribution to the impurity peaking related to the parallel impurity dynamics. For TE modes this contribution typically decreases the peaking factor, which is verified by quasilinear GYRO simulations. In the paper it is shown that the mode characteristics, and particularly the factor $\omega_r / \left(\omega_r^2 + \gamma^2\right)$, together with the safety factor are important for determining the magnitude of the parallel dynamics contribution. Moreover, for TE modes driven by the electron temperature gradient the peaking factor is found to be close to zero or negative, even in the poloidally symmetric case.

Paper D continues the work on the effect of poloidal asymmetries in the impurity density for axisymmetric plasmas. However, whereas the earlier papers focused on core transport in this work we study the pedestal at the edge of a plasma. From global neoclassical simulations it is shown that finite orbit width effects can cause a poloidal variation in the electrostatic potential, and that this poloidal variation can change substantially on a small radial scale. By gyrokinetic modelling of the radial turbulent impurity transport, we then show that these potential variations (both poloidal and radial) can significantly affect high-$Z$ impurity peaking. This model accounts for radial variations in the potential, appropriate in the plasma pedestal, and is thus an extension of the model in papers B and C.

In paper E we apply the previously developed theory to an experimental ICRH discharge in the Alcator C-Mod tokamak, which is an experiment well-suited to study high-$Z$ impurity transport. A clear ICRH-induced poloidal density asymmetry is present in the studied impurity species ($Mo^{32+}$) throughout the core region ($r/a \lesssim 0.6$) of the plasma in the discharge. Our theoretical model predicts a reduction in impurity peaking around mid radius, due to the poloidal asymmetries. However, the predicted peaking factor underestimates the experimentally observed very strong impurity peaking, which is so large that it must be induced by some mechanism not included in our gyrokinetic modelling. Pure neoclassical transport could be a candidate, but comparing the size of the fluxes from gyrokinetic simulations to neoclassical simulations shows that the turbulent transport is dominant. Still, it should be noted that uncertainties in atomic physics processes prevent quantitative comparison between modelling and experiment in this region of the plasma.

In papers F and G we direct our focus to 3D magnetic configurations. In 3D devices the neoclassical transport is predicted to constitute

a significant part of the radial transport, and often dominate over turbulent transport. Typically a strong neoclassical inward pinch of high-$Z$ impurities is expected, due to the presence of an ambipolar radial electric field. To make 3D devices attractive as a reactor concept it is of prime importance to be able to avoid strong impurity accumulation, and consequently it is a key task to predict neoclassical impurity transport.

We use the recently developed drift-kinetic solver, the SFINCS code described in Sec. 3.2.4, to analyze neoclassical impurity transport in W7-X plasmas. We also examine how impurities affect the bootstrap current in stellarators, which is important since a plasma current modifies the magnetic configuration and affects the confinement properties. In paper F we show that a very strong neoclassical peaking of high-$Z$ impurities could be expected in W7-X. This peaking is amplified by large pressure gradients of the main plasma species. In paper G the focus is instead on calculating neoclassical impurity transport coefficients in different collisionality regimes. We show that transport calculations should be performed with the full linearized Fokker-Planck operator, and that a pitch-angle scattering operator could lead to transport predictions in the wrong direction. Moreover, in both papers we show that a change in plasma effective charge of order unity can cause changes to the bootstrap current large enough to cause a deviation in the divertor strike point locations.

**Outlook** Future fusion reactors will have to use areas of high-$Z$ plasma facing materials to ensure sufficiently low wall erosion. In the current ITER design, tungsten has been chosen for the divertor, which faces the highest heat and particle loads, and the first wall will be covered by the lighter beryllium to minimize the effects of fuel dilution and radiative energy losses. To prepare for this, many tokamaks are installing tungsten plasma facing components (ASDEX Upgrade 2007, JET ITER-like wall 2011). Investigations into how central accumulation of high-$Z$ impurities may be avoided are thus timely and important. In this thesis we have analyzed the role of a poloidally varying non-fluctuating potential in impurity peaking caused by electrostatic microinstabilities, and demonstrated that this potential could affect the cross-field turbulent impurity transport considerably. Such a potential can arise e.g. when applying ICRH to a minority ion species on the low field side, and could be proposed as a method for mitigating impurity accumulation given that such heating systems are already an integral part of the ITER de-

sign.

Impurity accumulation is also one of the main dangers threatening the success of the stellarator approach. There has been very little theoretical modelling undertaken in the area of impurity transport in stellarators, and the optimal way to avoid impurity accumulation is not known. Due to the complicated 3D magnetic field structure these studies must be performed numerically. In this thesis we have used a novel drift-kinetic solver, SFINCS, to calculate neoclassical cross-field impurity fluxes. We have shown that strong impurity accumulation is indeed a concern for these devices, and also how the presence of impurities can affect the bootstrap current in 3D plasmas. A large parameter space remains to be explored, including the synergy of neoclassical and turbulent impurity transport and SFINCS will no doubt continue to be a useful tool in this endeavour.

# References


[1] Chen, F.F. *An Indispensable Truth: How Fusion Power Can Save the Planet*. Springer (2011). ISBN 978-1-4419-7819-6. http://dx.doi.org/10.1007/978-1-4419-7820-2.

[2] McCracken, G. and Stott, P. *Fusion: The energy of the Universe*. Elsevier Academic Press (2005). ISBN 0-12-481851-X.

[3] Freidberg, J. *Plasma Physics and Fusion Energy*. Cambridge University Press (2007). ISBN 978-0-521-73317-5.

[4] *All-the-World's Tokamaks*. www.tokamak.info.

[5] Romanelli, F. et al. *Fusion Electricity - EFDA*. Garching, Germany (2012). ISBN 978-3-00-040720-8.

[6] *ITER webpage*. http://www.iter.org/.

[7] Helander, P. and Sigmar, D.J. *Collisional transport in magnetized plasmas*. Cambridge University Press, Cambridge (2002). ISBN 978-0-521-80798-2.

[8] Wesson, J. *Tokamaks*. Clarendon Press, Oxford, third edition (2004). ISBN 978-0-19-850922-6. http://dx.doi.org/10.1088/0741-3335/46/3/173515.

[9] Kikuchi, M., Lackner, K. and Tran, M.Q. *Fusion physics*. International Atomic Energy Agency (2012). ISBN 978-92-0-130410-0. http://www-pub.iaea.org/books/IAEABooks/8879/Fusion-Physics.

[10] Helander, P. et al. Stellarator and tokamak plasmas: a comparison. Plasma Phys. Control. Fusion, **54** (2012), 124009. http://dx.doi.org/10.1088/0741-3335/54/12/124009.

[11] Helander, P. Theory of plasma confinement in non-axisymmetric magnetic fields. Rep. Prog. Phys., **77** (2014), 087001. http://dx.doi.org/10.1088/0034-4885/77/8/087001.

[12] Hirvijoki, E. Theory and models for Monte Carlo simulations of minority particle populations in tokamak plasmas. Ph.D. thesis, Aalto University (2014). http://urn.fi/URN:ISBN:978-952-60-5560-2.

[13] Chandrasekhar, S. Stochastic Problems in Physics and Astronomy. Rev. Mod. Phys., **15** (1943), 1. http://dx.doi.org/10.1103/RevModPhys.15.1.

[14] Rosenbluth, M.N., MacDonald, W.M. and Judd, D.L. Fokker-Planck Equation for an Inverse-Square Force. Phys. Rev., **107** (1957), 1. http://dx.doi.org/10.1103/PhysRev.107.1.

[15] Balescu, R. *Aspects of Anomalous Transport in Plasmas*. Institute of Physics Publishing (2005). ISBN 9780750310307.

[16] Braginskii, S.I. Transport Processes in a Plasma. Reviews of Plasma Physics, **1** (1965), 205.

[17] Hazeltine, R.D. Recursive derivation of drift-kinetic equation. Plasma Phys., **15** (1973), 77. http://dx.doi.org/10.1088/0032-1028/15/1/009.

[18] Angioni, C. et al. Density Peaking, Anomalous Pinch, and Collisionality in Tokamak Plasmas. Phys. Rev. Lett., **90** (2003), 205003. http://dx.doi.org/10.1103/PhysRevLett.90.205003.

[19] Landreman, M. et al. Comparison of particle trajectories and collision operators for collisional transport in nonaxisymmetric plasmas. Phys. Plasmas, **21** (2014), 042503. http://dx.doi.org/10.1063/1.4870077.

[20] Beidler, C.D. et al. Benchmarking of the mono-energetic transport coefficients–results from the International Collaboration on Neoclassical Transport in Stellarators (ICNTS). Nucl. Fusion, **51** (2011), 076001. http://dx.doi.org/10.1088/0029-5515/51/7/076001.

[21] Landreman, M. The monoenergetic approximation in stellarator neoclassical calculations. arXiv:1102.2508, (2011). http://arxiv.org/abs/1102.2508.

[22] Beer, M.A. Gyrofluid models of turbulent transport in tokamaks. Ph.D. thesis, Princeton University (1995).

[23] Candy, J. and Belli, E. GYRO Technical Guide. Technical report, General Atomics, San Diego, CA, USA (2014). https://fusion.gat.com/theory/Gyrodoc.

[24] Sugama, H. and Horton, W. Nonlinear electromagnetic gyrokinetic equation for plasmas with large mean flows. Phys. Plasmas, **5** (1998), 2560. http://dx.doi.org/10.1063/1.872941.

[25] Abel, I.G. et al. Multiscale gyrokinetics for rotating tokamak plasmas: fluctuations, transport and energy flows. Rep. Prog. Phys., **76** (2013), 116201. http://dx.doi.org/10.1088/0034-4885/76/11/116201.

[26] Connor, J.W., Hastie, R.J. and Taylor, J.B. Stability of general plasma equilibria. Plasma Physics, **22** (1980), 757–769. http://dx.doi.org/10.1088/0032-1028/22/7/013.

[27] Pusztai, I. Turbulent and Neoclassical Transport in Tokamak Plasmas. Ph.D. thesis, Chalmers University of Technology (2011). http://ft.nephy.chalmers.se/publications/pusztai_phd_thesis.pdf.

[28] Weiland, J. *Collective Modes in Inhomogeneous Plasma*. Institute of Physics Publishing (2000). ISBN 0750305894.

[29] Connor, J.W., Hastie, R.J. and Taylor, J.B. Shear, Periodicity, and Plasma Ballooning Modes. Phys. Rev. Lett., **40** (1978), 396–399. http://dx.doi.org/10.1103/PhysRevLett.40.396.

[30] Romanelli, F. and Briguglio, S. Toroidal semicollisional microinstabilities and anomalous electron and ion transport. Phys. Fluids B, **2** (1990), 754. http://dx.doi.org/10.1063/1.859313.

[31] Candy, J. and Waltz, R.E. An Eulerian gyrokinetic-Maxwell solver. J. Comput. Phys., **186** (2003), 545–581. http://dx.doi.org/10.1016/S0021-9991(03)00079-2.

[32] *GYRO webpage*. https://fusion.gat.com/theory/Gyro.

[33] Howard, N.T. et al. Quantitative comparison of experimental impurity transport with nonlinear gyrokinetic simulation in an Alcator C-Mod L-mode plasma. Nucl. Fusion, **52** (2012), 063002. http://dx.doi.org/10.1088/0029-5515/52/6/063002.

[34] Valisa, M. et al. Metal impurity transport control in JET H-mode plasmas with central ion cyclotron radiofrequency power injection. Nucl. Fusion, **51** (2011), 033002. http://dx.doi.org/10.1088/0029-5515/51/3/033002.

[35] Reinke, M.L. et al. Poloidal variation of high-Z impurity density due to hydrogen minority ion cyclotron resonance heating on Alcator C-mod. Plasma Phys. Control. Fusion, **54** (2012), 045004. http://dx.doi.org/10.1088/0741-3335/54/4/045004.

[36] Ingesson, L.C. et al. Comparison of basis functions in soft x-ray tomography and observation of poloidal asymmetries in impurity density. Plasma Phys. Control. Fusion, **42** (2000), 161–180. http://dx.doi.org/10.1088/0741-3335/42/2/308.

[37] Ye. O. Kazakov et al. Poloidal asymmetries due to ion cyclotron resonance heating. Plasma Phys. Control. Fusion, **54** (2012), 105010. http://dx.doi.org/10.1088/0741-3335/54/10/105010.